ISSN 0386-4049

気象研究所技術報告 第六十六号

TECHNICAL REPORTS OF THE METEOROLOGICAL RESEARCH INSTITUTE No.66

A method forestimating the sea-air CO_2 flux in the Pacific Ocean

BY

Hiroyuki Sugimoto, Naotaka Hiraishi,
Masao Ishii, Takashi Midorikawa

気象研究所技術報告
第 66 号
太平洋における大気－海洋間二酸化炭素フラックス推定手法

杉本裕之，平石直孝，石井雅男，緑川　貴

気象研究所

METEOROLOGICAL RESEARCH INSTITUTE, JAPAN

February 2012

TECHNICAL REPORTS OF THE MRI, NO.66

The *Technical Reports of the Meteorological Research Institute* has been issued at irregular intervals by the Meteorological Research Institute (MRI) since 1978 as a medium for the publication of technical report including methods, data and results of research, or comprehensive report compiled from published papers. The works described in the *Technical Reports of the MRI* have been performed as part of the research programs of MRI.

太平洋における大気－海洋間二酸化炭素フラックス推定手法

A method for estimating the sea-air CO_2 flux in the Pacific Ocean

杉本裕之

気象庁地球環境・海洋部／気象研究所海洋研究部

平石直孝

気象庁地球環境・海洋部（現：気象庁観測部）

石井雅男，緑川　貴

気象研究所地球化学研究部

Hiroyuki Sugimoto

Global Environment and Marine Department, Japan Meteorological Agency

Ocean Research Department, Meteorological Research Institute

Naotaka Hiraishi

Global Environment and Marine Department, Japan Meteorological Agency

(Present Affiliation; Observations Department, Japan Meteorological Agency)

Masao Ishii, Takashi Midorikawa

Geochemical Research Department, Meteorological Research Institute

序　文

産業革命以後、人類は化石燃料の消費や森林伐採などによって、大量の二酸化炭素（CO_2）を大気中に排出してきた。これによって引き起こされている大気中の CO_2 濃度の著しい増加や地球温暖化に、今、大きな関心が社会から寄せられている。海洋は、産業革命以後に排出された人為起源 CO_2 のおよそ半分を吸収してきたと推定されており、大気中の CO_2 増加を緩和して温暖化を抑制する重要な役割を担っている。しかしながら、近年、人為起源 CO_2 の排出量がますます増加しているにも関わらず、海洋がこれを吸収する割合は減少しているとの指摘もある。今後、地球温暖化の予測精度を向上させてゆくためには、海洋が大気中から CO_2 を吸収する速度やメカニズムについて、より深く理解することが不可欠となっている。

近年、海洋でも、CO_2 分布の観測が精力的に行われている。国際協力によって観測データのデータベース化も進められており、海水中の CO_2 分圧や大気－海洋間の CO_2 フラックスの分布も月ごとに評価されている。しかし、それらは気候値的な分布の評価にとどまっており、気象や海況変動の影響による様々な時間スケールの変動は、よく分かっていない。数値モデルなどを使った全球や海域ごとの CO_2 フラックスの評価も行われているが、その結果は、用いたモデルやモデルを駆動する強制力などによって大きく異なっており、より多くの実測データに基づいた、より信頼性の高い評価が求められている。海水中の CO_2 分圧の変動特性を実測し、これを利用して大気－海洋間の CO_2 フラックスを経験的に見積もる手法も開発されてきた。しかしながら、こうした経験的な手法が適用できる海域も、これまではいくつかの海域に限られていた。

本技術報告では、統合された海洋 CO_2 分圧のデータベースを利用して、北太平洋と南太平洋の広域における CO_2 分圧の面的分布を、長い期間にわたって月ごとに評価する新たな経験的手法について紹介する。これを衛星データや大気再解析データなどと組み合わせて活用することで、観測の空白時期・海域を含む広い領域について CO_2 フラックスを評価でき、今後も海洋が人為起源 CO_2 を多く吸収し続けるのかどうか、大気中の CO_2 増加に対して海洋が果たす役割の変化を評価する上で、大いに役立つものと期待される。

気象研究所
地球化学研究部長
緑　川　　貴

Preface

Since the industrial revolution, the release of carbon dioxide (CO_2) from the activities of humankind, such as fossil-fuel combustion and land-use change, has dramatically increased atmospheric CO_2 concentrations leading to significant recent global warming. The ocean has absorbed about half of the anthropogenic carbon emissions over the industrial era. This absorption has benefited humankind by reducing the growth of CO_2 levels in the atmosphere and consequently decelerating global warming. Recent reports have indicated a decline in the efficiency of the ocean as a carbon sink for anthropogenic emissions under increasing atmospheric CO_2 levels in recent years. To precisely predict future global warming, it is essential to understand the ocean carbon sink.

Recent extensive observations of oceanic CO_2 and international synthesis of global data have resulted in the production of a map of the monthly climatological partial pressure of CO_2 (pCO_2) in surface waters and the estimation of the global ocean CO_2 uptake. These studies provided a climatological mean field of the ocean carbon sink, but the variability of this sink at various time-scales remains poorly understood. Estimates of global and regional ocean carbon sinks by using ocean models are generally controversial, depending on the model and method. Therefore, observational data are required for realistic evaluation of ocean carbon sinks. Empirical methods have been developed in several regions of the ocean to evaluate the regional CO_2 flux by using the characteristics of oceanic pCO_2 fluctuations. However to date the regions where such empirical methods can be applied are limited.

In this technical report, we describe a newly developed method for evaluating monthly fields of oceanic pCO_2 and the subsequent temporal variations of the sea-air CO_2 flux over extensive regions of the North and South Pacific by using synthesized observational data. The application of this method is expected to contribute to understanding of future changes in the ocean carbon sink and the ocean's role in controlling the rate of atmospheric CO_2 increase.

Takashi Midorikawa, PhD.
Director of Geochemical Research Department
Meteorological Research Institute

要　旨

表面海水中の二酸化炭素分圧 (pCO_2s) と海面水温 (SST) 等のパラメータとの関係を利用して、太平洋における pCO_2s および大気－海洋間の二酸化炭素フラックスの月ごとの分布を推定する経験的手法を開発した。本手法では SST だけでなく、リモートセンシングやデータ同化によって得られた海面塩分（SSS）と海面クロロフィル濃度（Chl-a）も用いた。特に、高緯度域は、無機炭素の生物消費がブルーミングの時期に多くなる海域で、Chl-a を導入することによって pCO_2s の推定バイアスが改善された。太平洋全体での pCO_2s の推定バイアスは −10〜+10 μatm である。

この経験的手法を用いて 1985〜2009 年の月ごとの二酸化炭素フラックスを推定した。中緯度帯の冬季は、多量の二酸化炭素吸収が見られる。対照的に、赤道域では、大気への二酸化炭素の放出が一年中起きている。赤道域の二酸化炭素フラックスはエルニーニョ・南方振動(ENSO)とともに変動する。二酸化炭素の放出量はエルニーニョ現象の発生期間中（ENSO warm phase）に減少し、ラニーニャ現象の発生期間中（ENSO cold phase）に増加する。南緯 50 度以北の太平洋で、年積算した二酸化炭素フラックスの平均値は−0.59 ± 0.14 PgC yr^{-1}（負値は海洋が吸収することを示す）と推定された。本手法で推定された平均吸収量は Takahashi *et al.*(2009) によって見積もられた気候値（−0.46 PgC yr^{-1}）と比べて多く、主にガス交換係数の違いによるものであった。

二酸化炭素フラックスは、その計算に用いたガス交換係数の計算式や高さ 10m の風速（U_{10}）に大きな影響を受ける。そのため、3 種類のガス交換係数計算式と 3 種類の大気解析データを利用して二酸化炭素フラックスの違いを評価した。異なるガス交換係数計算式を使って計算した二酸化炭素フラックスは 15〜20%の違いがあった。NCEP/NCAR Reanalysis I で計算した二酸化炭素フラックスは主に赤道域で有意に小さく、JRA25/JCDAS で計算した二酸化炭素フラックスとの違いはおよそ −0.12 PgC yr^{-1}（20%）であった。

Abstract

We developed an empirical method for estimating monthly fields of the carbon dioxide (CO_2) partial pressure in surface seawater (pCO_2s) and the sea-air CO_2 flux in the Pacific Ocean by using the relationships between pCO_2s and other parameters. The method uses not only sea surface temperature (SST) but also sea surface salinity (SSS) and chlorophyll-*a* concentration (Chl-*a*) derived by remote sensing and data assimilation. The introduction of Chl-*a* data significantly reduces the estimation bias especially for the high latitudes where net biological uptake of inorganic carbon is very high during the bloom season. The bias in pCO_2s estimates throughout the Pacific is between −10 and +10 μatm.

We used our empirical method to estimate the monthly CO_2 flux with a resolution of 1° × 1° from 1985 through 2009. The uptake of CO_2 by the ocean is high in the mid-latitudes in winter. In contrast, CO_2 is released to the atmosphere throughout the year in the equatorial region. The CO_2 outflux in the equatorial region varies with El Niño/Southern Oscillation (ENSO). The emission of CO_2 decreases during El Niño (ENSO warm phase) and increases during La Niña (ENSO cold phase). The mean annual CO_2 flux in the Pacific north of 50°S was estimated at −0.59 ± 0.14 PgC yr^{-1} (a negative value indicates uptake by the ocean). This value is greater than the climatological value (−0.46 PgC yr^{-1}) determined by Takahashi *et al*. (2009b) mainly due to the difference in gas transfer coefficients used in the studies.

The estimate of CO_2 flux largely depends on the gas transfer coefficient and wind speed at 10 m above sea level (U_{10}) used in the calculations. Therefore we also evaluated the differences in CO_2 flux estimates based on three gas transfer coefficient formulas and three data sets for U_{10}. The CO_2 fluxes calculated with different equations of gas transfer coefficients differed by 15–20%. The CO_2 flux calculated using data from National Centers for Environmental Prediction-National Center for Atmospheric Research (NCEP/NCAR) Reanalysis I is significantly lower in the equatorial region than that calculated with Japanese 25-year Reanalysis/JMA Climate Data Assimilation System (JRA25/JCDAS) data; the mean difference is about −0.12 PgC yr^{-1}, or about 20%.

Contents

1. Introduction

Currently, the global oceans are considered to be absorbing about 30% of the carbon dioxide (CO_2) released by fossil-fuel combustion (IPCC, 2007). However, where and how the CO_2 is absorbed from the atmosphere into the oceans and how this absorption changes with time are largely unknown. It is important to assess the sea-air CO_2 flux and its detailed spatiotemporal variation over the global oceans with minimal uncertainty to understand the ocean carbon cycle and its controlling processes. This will help to reduce the uncertainty of predicted future atmospheric CO_2 concentrations and to improve projections of global warming.

Data for the CO_2 partial pressure in surface seawater (pCO_2s) are necessary for calculating the sea-air CO_2 flux. To date, millions of pCO_2s data have been acquired (Takahashi et al., 2008). However, pCO_2s is extremely variable in space and time. To document the changes in pCO_2s and sea-air CO_2 flux at basin to global scales with sufficient temporal resolution, it is necessary to fill in the spatial and temporal gaps in the data.

Takahashi et al. (1993, 2002, 2009b) have estimated the climatological monthly pCO_2s by using a time-space interpolation of pCO_2s data. In this method, pCO_2s data are first corrected to those in a reference year using the rate of increase in atmospheric CO_2 concentration, and then a climatological pCO_2s distribution is constructed by interpolation based on a lateral two-dimensional advection-diffusion model. However, this method does not account for the influences of year-to-year and decadal variations such as those associated with the El Niño/Southern Oscillation (ENSO) and the Pacific Decadal Oscillation (PDO).

Empirical methods using the relationships between pCO_2s and other parameters such as sea surface temperature (SST) and salinity (SSS) have been developed to deduce year-to-year variability. For example, Park et al. (2010) estimated global pCO_2s by using pCO_2s-SST relationships. The Japan Meteorological Agency (JMA) has provided CO_2 flux information for the subtropical western North Pacific annually since 1999, and for the equatorial Pacific since 2007, by using empirical analysis methods based on SST-pCO_2s and SSS-pCO_2s relationships (Murata et al., 1996; Nakadate and Ishii, 2007). However, these simple methods are insufficient for representing the drawdown of pCO_2s due to biological CO_2 uptake, such as in the subpolar regions, and there are areas for which there are insufficient data to develop an accurate empirical method. Therefore, the area for which JMA provides CO_2 flux estimates has been limited to only about 1/12 of the global ocean. Improvements in the empirical method are required to expand the estimation area to the global ocean.

Recently, remote sensing data for chlorophyll-*a* concentrations (Chl-*a*) from satellites have become available, and these data are also used in empirical methods to represent the pCO_2s drawdown due to biological CO_2 uptake (Ono et al., 2004; Sarma et al., 2006; Chierici et al., 2009). In addition, the database of global pCO_2s has been revised (Takahashi et al., 2008). In this study, we develop an empirical method to estimate pCO_2s in the Pacific by generating equations from multiple regression analysis between pCO_2s and other parameters, including Chl-*a*. These relationships vary regionally. We divided the Pacific Ocean into smaller regions for the multiple regression analyses so that the pCO_2s in each region could be expressed by a single relationship between pCO_2s and other parameters. The estimation biases were no more than ±10 μatm

as confirmed by comparison with observational data (Takahashi et al., 2009a). The inclusion of Chl-*a* data significantly reduces the estimation errors in the subpolar areas, which have intense biological activity.

In addition, we calculated the monthly pCO_2s and CO_2 flux in the Pacific for the past 25 years (1985–2009). We calculated the monthly CO_2 flux by using different combinations of gas transfer coefficient equations and three data sets of wind speed at 10 m above sea level (U_{10}) to evaluate the uncertainty.

We describe the target region and data sets used in this study in section 2. The method of pCO_2s estimation, including the partitioning of the region and the multiple regression analysis, is presented in section 3. In section 4, we discuss the estimation of pCO_2s and its error. Finally, in section 5 we provide seasonal maps and time series of the CO_2 flux, investigate the effects of the choice of gas transfer coefficient equations and U_{10} data sets on the flux estimates, and compare our mean CO_2 flux values with the climatological values presented by Takahashi et al. (2009b).

2. Target region and data

Our target region is shown in Fig. 1. This region contains most of the Pacific Ocean except for the marginal seas (Japan Sea, Yellow Sea and Bering Sea). Because the seasonal variation of pCO_2s is different in different parts of the Pacific, we divided the targeted study area into five smaller regions. The thermodynamic effect dominates the variation in pCO_2s in the North and South Pacific subtropical regions (NP/T and SP/T, respectively; Murata et al., 1996; Takahashi et al., 2002). Upwelling elevates pCO_2s in the equatorial region (EQ; Nakadate and Ishii, 2007; Feely et al., 2006) and the carbon supplied through vertical mixing in winter, and carbon consumption by phytoplankton from spring to autumn affect the subarctic and subantarctic regions (NP/A and SP/A respectively; Ono et al., 2004; Sarma et al., 2006; Takahashi et al., 2002).

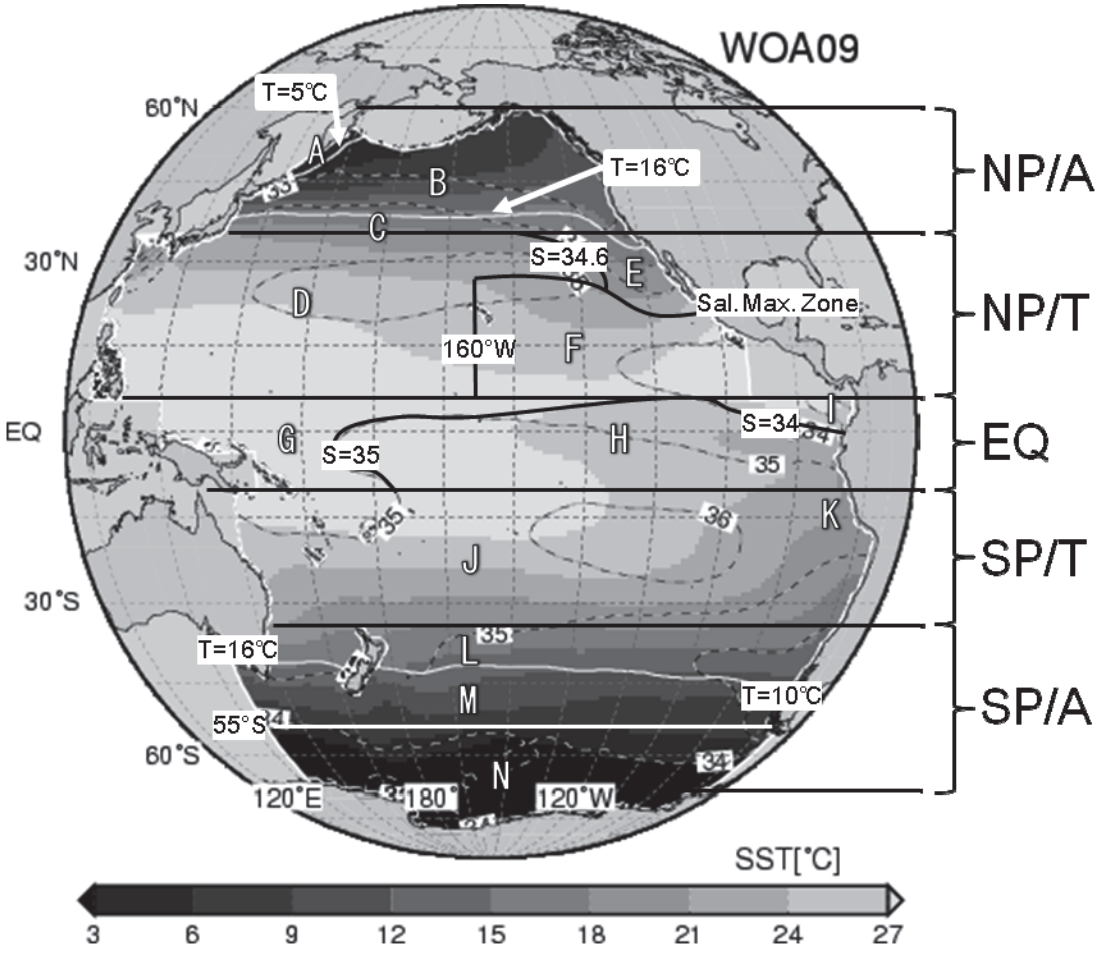

Figure 1. Annual mean SST (shading) and SSS (broken lines) climatology from the World Ocean Atlas 2009 (WOA09; SST, Locarnini et al. [2010]; SSS, Antonov et al. [2010]). NP/A, subarctic North Pacific; NP/T, subtropical North Pacific; EQ, Equatorial Pacific; SP/T, subtropical South Pacific; SP/A, subantarctic South Pacific (see sections 3 and 4). Solid lines delineate 14 smaller regions A–N.

We used the Lamont-Doherty Earth Observatory (LDEO) Database V1.0 (Takahashi et al., 2008) for pCO_2s analysis. This database consists of about 3.5 million pCO_2s measurements collected between 1968 and 2006. There are relatively more pCO_2s measurements from the equatorial and North Pacific and fewer

from the South Pacific.

We used several gridded datasets to estimate pCO_2s and CO_2 flux (Table 1). We used the "Merged satellite and in situ data Global Daily Sea Surface Temperatures" (MGDSST; Kurihara et al., 2006) dataset, analyzed by JMA. SSS was analyzed by the Multivariate Ocean Variational Estimation System/Meteorological Research Institute Community Ocean Model (MOVE/MRI.COM-G; Usui et al., 2006) developed by JMA/MRI. The Chl-*a* fields used are monthly level-3 standard maps of SeaWiFS and MODIS-Aqua data prepared by the National Aeronautics and Space Administration/Goddard Space Flight Center/Distributed Active Archive Center (NASA/GSFC/DAAC; Feldman and McClain, 2010a and 2010b) and downloaded from the Ocean Color Home Page (http://oceancolor.gsfc.nasa.gov/). Monthly sea level pressure (SLP) and U_{10} fields are from the Japanese 25-year Reanalysis/JMA Climate Data Assimilation System (JRA25/JCDAS; Onogi et al., 2007). The atmospheric CO_2 concentrations from JMA were from model calculations using an inversion method based on data reported to the World Data Centre for Greenhouse Gases (WDCGG) (Maki et al., 2010).

As monthly remotely sensed Chl-*a* are not available before 1997, we used monthly Chl-*a* climatology to estimate pCO_2s and CO_2 flux between 1985 and 1997. Because these data sets differ in their horizontal resolution, we used linear interpolation or areal mean values to generate a dataset with 1° × 1° resolution.

Table 1. Gridded datasets used in this study.

Variable	Data	Resolution (longitude × latitude)	Reference
SST	MGDSST	0.25° ×0.25°	Kurihara et al.(2006)
SSS	MOVE/MRI.COM-G	1.0° ×0.3° ～1.0°	Usui et al.(2006)
Chl-a	SeaWiFS Reprocessing 2009.1 / MODIS-Aqua Reprocessing 2009.1	1/12° ×1/12°	Feldman and McClain (2010a, 2010b)
SLP	JRA25(1985-2004)/ JCDAS(2005-2008)	1.25° ×1.25°	Onogi et al.(2007)
10m wind speed			
xCO_2a	Carbon dioxide (CO_2) destribution	2.5° ×2.5°	Maki et al.(2010)

3. Method for estimating pCO_2s

3.1. Correction for long-term trends

Since the 1960s, pCO_2s has been increasing in response to increasing CO_2 partial pressure in air (pCO_2a) (Inoue et al., 1999; Inoue and Ishii, 2005; Takahashi et al., 2009b). In order to develop a method to estimate pCO_2s by multiple regression, it is necessary to take into account these long-term trends.

In the subtropical North Pacific (excluding the southeastern portion; area 'F' in Fig. 1) and in the equatorial region where pCO_2s has been regularly observed, pCO_2s data are available with dense coverage in both space and time. Here, the long-term trends of pCO_2s can be evaluated by including the time of the observation as one of the terms in the multiple regression analysis.

In the subarctic and the southeastern subtropical North Pacific, the number of pCO_2s observations has been increasing recently, but in the past the data were few. In the South Pacific data are particularly sparse. Therefore, including the time of observations in the regression analysis does not properly determine long-term trends. Here, we investigated long-term trends of CO_2 concentrations in surface seawater (xCO_2s) in each 1° zonal band in these regions by selecting the areas and seasons for which there were sufficient data (Fig. 2a [lower] and 2b). We determined the latitudinal distributions of xCO_2s since 1969 and the latitudinal variation in the annual rate of increase of xCO_2s (Fig. 2a [upper]).

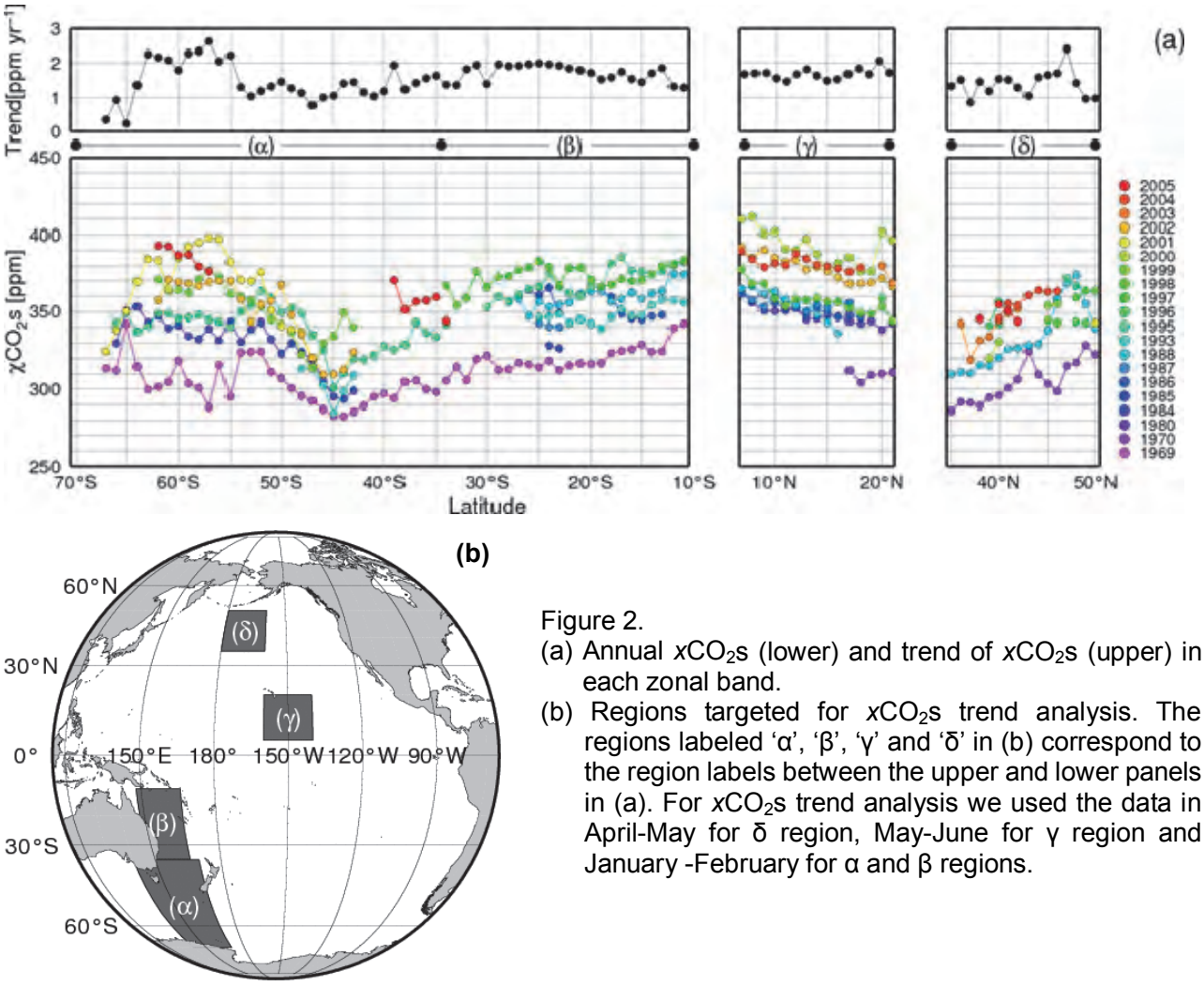

Figure 2.
(a) Annual xCO_2s (lower) and trend of xCO_2s (upper) in each zonal band.
(b) Regions targeted for xCO_2s trend analysis. The regions labeled 'α', 'β', 'γ' and 'δ' in (b) correspond to the region labels between the upper and lower panels in (a). For xCO_2s trend analysis we used the data in April-May for δ region, May-June for γ region and January -February for α and β regions.

In the subarctic North Pacific (region δ in Fig. 2b) the rates of increase range from 0.9 to 2.4 ppm yr^{-1} (average ± SD, 1.4 ± 0.4 ppm yr^{-1}). In the subtropical region (β) and (γ), the rates of increase are fairly constant with small variation; the average in both of these subtropical regions is 1.7 ± 0.2 ppm yr^{-1}. In the subantarctic South Pacific (α), the rate of increase varies from north to south. Between the subtropical front (55°S) and the subantarctic front (63°S), the rates exceed 2.0 ppm yr^{-1}. At lower latitudes (north of 55°S), the rates are 1.0 to 1.5 ppm yr^{-1}, and at higher latitudes (south of 63°S) the rates are very low. This characteristic distribution in the subantarctic South Pacific was also reported by Inoue and Ishii (2005). The average rates in this study are 1.3 ± 0.3 ppm yr^{-1} (35°S–54°S) and 2.2 ± 0.2 ppm yr^{-1} (55°S–63°S). We prepared multiple regression equations for these data-sparse regions by using the available data corrected to the year 2000 by the respective average rates of change.

3.2. Empirical method for estimating CO_2 concentration in surface seawater.

We generated acceptable empirical equations for estimating xCO_2s in each region by performing multiple regression analysis based on the relationships between SST, SSS and xCO_2s in each region (Fig. 3). Because xCO_2s varies primarily because of the thermodynamic effect from changes in temperature and salinity, we examined relationships between SSS and xCO_2s by using CO_2 data normalized to 10°C (n-xCO_2s) by using an empirical equation of Takahashi et al. (1993).

3.2.1. The subtropical region

We found a positive linear relationship between SST and xCO_2s in the subtropical region. This relationship results from the thermodynamic effect of temperature, which plays a dominant role in the variation of xCO_2s because of the shallow mixed layer and scarce nutrients (Murata et al., 1996; Takahashi et al., 2002; Park et al., 2010). Higher xCO_2s is observed in seasons with higher SST and lower xCO_2s in seasons with lower SST.

An exception is found off the coast of Peru where upwelling occurs. Coastal upwelling supplies inorganic carbon, causing higher xCO_2s in austral winter and spring. Thus the region off Peru becomes a source of atmospheric CO_2 (Friederich et al., 2008).

3.2.1.a. The North Pacific (NP/T)

In the western subtropical region (west of 160°W), there are robust linear relationships between SST and xCO_2s (red oval in Fig. 3b). xCO_2s can be estimated with small uncertainty by a linear regression with SST as reported by Murata et al. (1996). JMA observes xCO_2s along 137°E and 165°E each season as part of operations from on board the research vessels *Ryofu-Maru* and *Keifu-Maru*. Linear regression equations can be determined annually for each 1° (latitude) × 1° (longitude) grid by using these data.

In the eastern subtropical region (east of 160°W), the meridional SSS maximum is observed along about 20°N (Fig. 1). There is a negative linear relationship between n-xCO_2s and SSS north of the salinity maximum (blue oval in Fig. 3g) and a positive linear relationship south of the maximum (green oval in Fig. 3g). For this reason, we separated the northern region from the southern by the salinity maximum in the eastern subtropical North Pacific, and determined multiple regression equations with SST, SSS and year for

each region as

$$xCO_2s = 400.75 + 9.92 \cdot T_{25} - 21.26 \cdot S_{35} + 1.14 \cdot Yr_{2000} \quad (\pm \text{SE}, \pm 14.5) \qquad (1)$$

for Region E (northeastern subtropical region; north of the SSS maximum and SSS < 34.6), and

$$xCO_2s = 364.73 + 7.99 \cdot T_{25} + 12.56 \cdot S_{35} + 1.7 \cdot Yr_{2000} \quad (\pm 14.9) \qquad (2)$$

for Region F (southeastern subtropical region; south of the SSS maximum).
T_{25}, S_{35} and Yr_{2000} are [SST − 25], [SSS − 35] and [year − 2000], respectively. For the rest region (north of the SSS maximum and SSS ≥ 34.6) we used the same equation as that for Region D.

3.2.1.b. The South Pacific (SP/T)

Positive linear relationships were found between SST and xCO$_2$s in almost all regions of the subtropical South Pacific except for off Peru (Region J; green oval in Fig. 3d). The value for xCO$_2$s at SST = 25 °C from the linear regression gradually increases toward the east.

Off the coast of Peru, there is a negative linear relationship between SST and xCO$_2$s because of the influence of coastal upwelling (Region K; blue oval in Fig. 3d). This relationship is found only north of 20°S and east of 95°W from July to December. This region during this season is called the "coastal upwelling region". In contrast, there are no clear relationships between SSS and n-xCO$_2$s throughout the entire subtropical region (Fig. 3i).

We calculated a climatological linear regression equation for the relationship between SST and xCO$_2$s for each 1° × 1° grid by using the xCO$_2$s data corrected to the year 2000, and produced an empirical equation by adding the long term trend estimated in section 3.1 (1.7 ppm yr^{-1}) to this climatological equation for Region J:

$$xCO_2s = A(Lon, Lat) + B(Lat) \cdot T_{25} + 1.7 \cdot Yr_{2000} \qquad (3)$$

A and B are intercept and slope, respectively. Slope B is calculated for each 1° zonal band by using observational data between 170°E and 170°W. The intercept A is the xCO$_2$s at SST = 25 °C, corrected using the slope B.

In the coastal upwelling region, the linear relationship between SST and xCO$_2$s changes with latitude, because the upwelling strengthens toward the north. Therefore, we calculated a linear regression equation for each 1° zonal band in Region K:

$$xCO_2s = A'(Lat) + B'(Lat) \cdot T_{25} + 1.7 \cdot Yr_{2000} \qquad (4)$$

where A' and B' are intercept and slope, respectively.

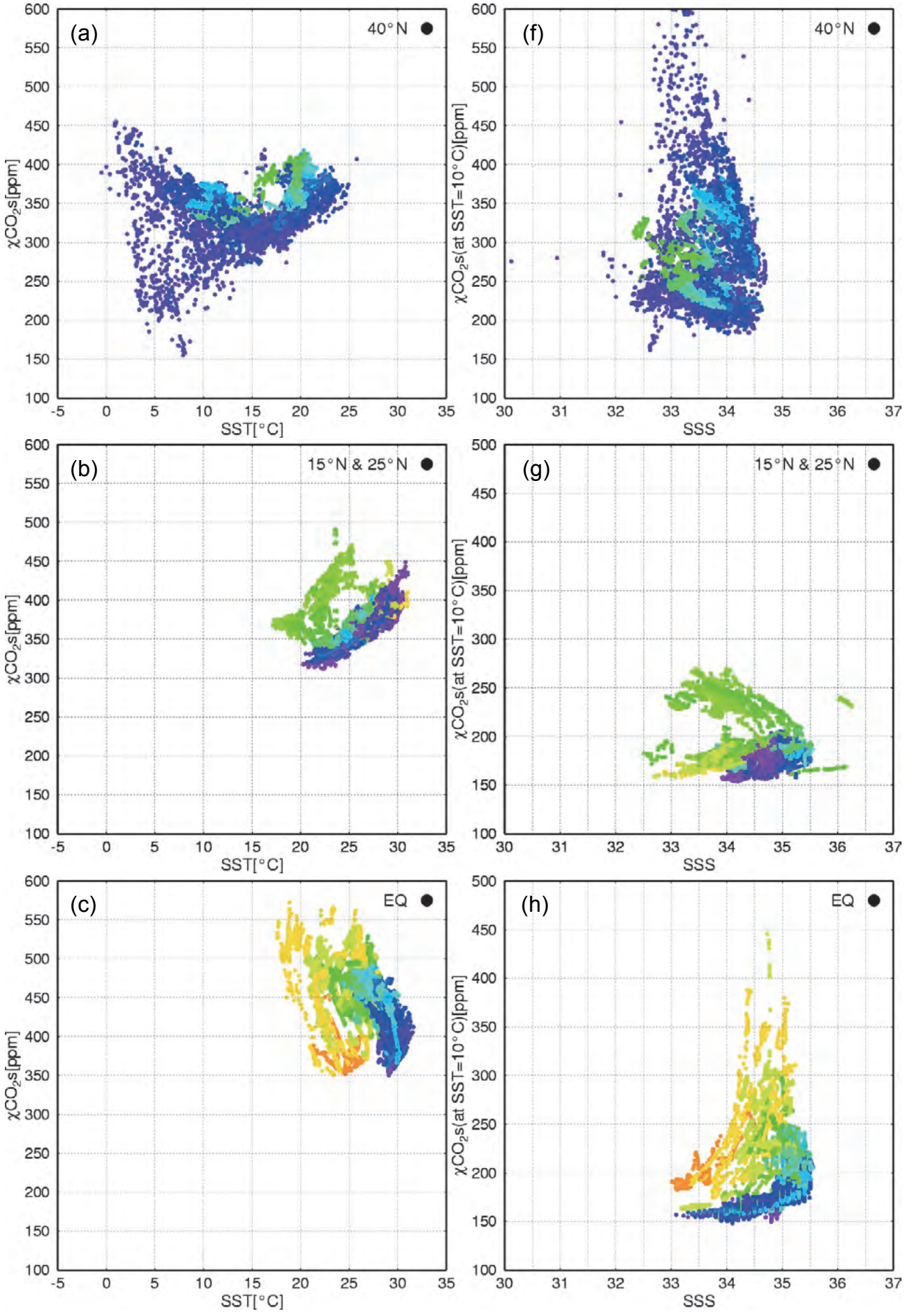
(a)
40°N
(b)
15°N & 25°N
(c)
EQ
(f)
40°N
(g)
15°N & 25°N
(h)
EQ
χCO2s[ppm]
χCO2s(at SST=10°C)[ppm]
SST[°C]
SSS

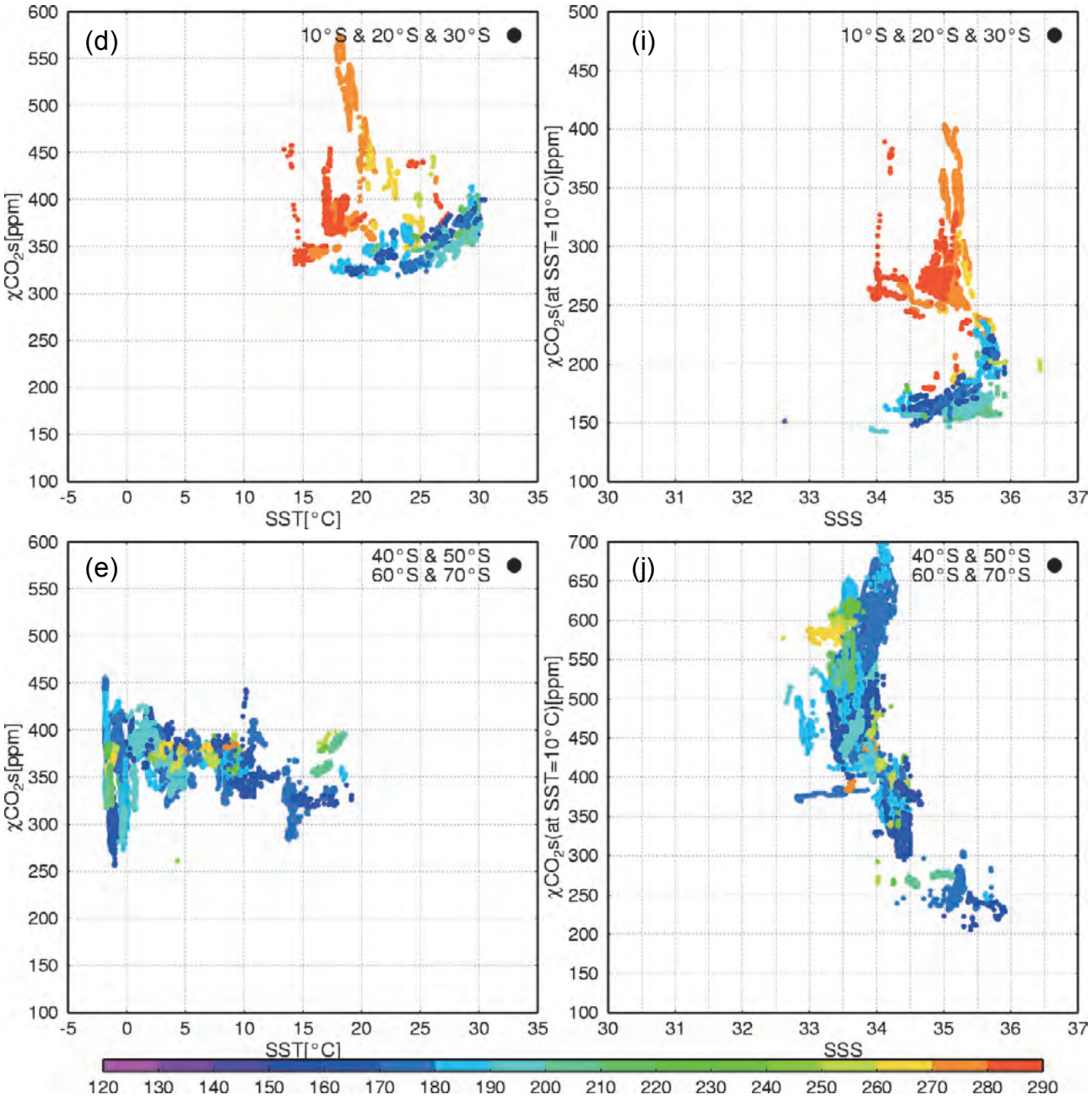

Figure 3. Relationships between xCO_2s and SST (left column) or SSS (right column) in five regions of the Pacific Ocean: (a) and (f), NP/A; (b) and (g), NP/T; (c) and (h), EQ; (d) and (i), SP/T; (e) and (j), SP/A. The labels “Positive” or “Negative” indicate the signs of the regression coefficients between xCO_2s and SST or SSS.

3.2.2. The equatorial region (EQ)

The easterly trade winds cause equatorial upwelling. This upwelling brings cold and carbon-rich water from deeper layers to the surface. In the equatorial region, SST and $x\mathrm{CO_2}$s are negatively correlated and this relationship varies seasonally and annually. Cosca et al. (2003) and Feely et al. (2006) used this relationship to derive seasonal and inter-annual equations for estimates of $p\mathrm{CO_2}$s. In contrast, Nakadate and Ishii (2007) and Ishii et al. (2009) used SSS to divide the equatorial region into the warm pool region and the upwelling region and derived two equations to calculate $x\mathrm{CO_2}$s. In this region ENSO determines the strength of upwelling and the wind patterns, which cause inter-annual variation of $\mathrm{CO_2}$ flux (Cosca et al., 2003; Feely et al., 2006; Nakadate and Ishii, 2007; Ishii et al., 2009).

In the equatorial upwelling region, we found a negative linear relationship between SST and $x\mathrm{CO_2}$s that varies seasonally, as reported by Cosca et al. (2003) and Feely et al. (2006) (blue oval in Fig. 3c). The relationship between SSS and n-$x\mathrm{CO_2}$s is a quadric convex distribution and n-$x\mathrm{CO_2}$s reaches a peak at SSS = 35 (blue oval in Fig. 3h).

The warm-pool region spreads to the west of the upwelling region where there is a positive linear relationship between SST and $x\mathrm{CO_2}$s. The relationship between SSS and n-$x\mathrm{CO_2}$s is not clear in this region (red oval in Fig. 3c and 3h). East of the upwelling region, SSS and $x\mathrm{CO_2}$s are relatively low (green oval in Fig. 3c and 3h). A positive relationship between SSS and n-$x\mathrm{CO_2}$s is seen in this region where SSS is above 34.

On the basis of these observations, we divided the equatorial region into three sub-regions: the warm pool region (G), the upwelling region (H) and the low salinity region (I). The geographic distribution of these three sub-regions varies with time depending on the distribution of SSS. The boundary between the upwelling region and the other two regions is defined by the following relationship:

$$SSS_{bnd} = \begin{cases} 35 & (\text{west of } 160^\circ\text{W}) \\ 35 + \dfrac{lon - 160}{40} & (\text{between } 160^\circ\text{W and } 120^\circ\text{W}) \\ 34 & (\text{east of } 120^\circ\text{W}) \end{cases} \qquad (5)$$

where '*lon*' indicates longitude in degrees west. The area where SSS $\geq SSS_{bnd}$ is classified as the upwelling region (Region H) and the region where SSS $< SSS_{bnd}$ contains the other two sub-regions. The area where SSS $< SSS_{bnd}$ is divided into two smaller regions at 140°W. The area west of 140°W is regarded as the warm pool region (Region G) and east of 140°W is the low salinity region (Region I).

Eq. 6 below is the empirical formula for the distribution of $x\mathrm{CO_2}$s in the equatorial region. We used a quadratic expression because of the quadric convex relationship between SSS and n-$x\mathrm{CO_2}$s in the upwelling region (blue oval in Fig. 3h). A sine-function term for the month ("*Mn*" in Eq. 6; 1 to 12 for January through December, respectively) is added to the equation only in the upwelling region to express the seasonal variation.

$$x\mathrm{CO_2s} = a + b \cdot T_{25} + c \cdot S_{35} + d \cdot {T_{25}}^2 + e \cdot {S_{35}}^2 + f \cdot T_{25} \cdot S_{35} + g \cdot Yr_{2000} + h \cdot \sin\left[2\pi \frac{Mn - i}{12}\right] \qquad (6)$$

The coefficients and root mean square errors (RMSEs) for each region are listed in Table 2.

Table 2. Coefficients and RMSEs for the multiple regression Eq. 5 for each sub-region in the equatorial Pacific (EQ). Letters after sub-region names correspond to the region codes in Figure 1.

Region	*a*	*b*	*c*	*d*	*e*	*f*	*g*	*h*	*i*	*RMSE* ppm
Warm pool (G)	455.76	-21.65	65.11	1.70	4.97	-8.18	1.97	—	—	12.6
Divergence area (H)	465.95	-10.51	9.29	-0.49	-66.86	2.86	1.31	14.87	0.40	27.4
Low salinity (I)	423.30	-1.23	53.56	0.65	8.51	-2.18	1.50	—	—	15.8

3.2.3. The subpolar regions

In the subpolar regions, strong vertical mixing supplies inorganic carbon from deep cold waters each winter. The increase in xCO_2s by vertical mixing exceeds xCO_2s reduction by seasonal cooling. There is a negative relationship between SST and xCO_2s in this region (Takahashi et al., 1993; Park et al., 2006).

In addition, phytoplankton consumes inorganic carbon in spring, with more consumption in the western North Pacific. To estimate the carbon reduction, previous studies have used Chl-*a* levels measured by remote sensing (Ono et al., 2004; Sarma et al., 2006; Chierici et al., 2009). In general, Chl-*a* is negatively correlated with xCO_2s because more carbon is consumed when more Chl-*a* is observed.

3.2.3.a The North Pacific (NP/A)

There is a positive linear relationship between SST and xCO_2s in the region of the subarctic North Pacific where SST ≥ 16 °C, as was also seen in the subtropical region (red oval in Fig. 3a). In this region, nutrients are exhausted and xCO_2s mainly varies from the thermodynamic effect. The intercept of the linear regression at 25 °C gradually increases toward the east. There is a negative relationship between SSS and n-xCO_2s in this region (red oval in Fig. 3f; referred as 'the northern subtropical region' (defined later)), with SSS increasing from west to east.

In the open ocean where SST < 16 °C and west of 160°E, there is a negative linear relationship between SST and xCO_2s (blue and orange ovals in Fig. 3a) and no significant relationship between SSS and n-xCO_2s.

In the region where 5 °C ≤ SST < 16 °C, the slope of the linear regression between SST and xCO_2s in summer (from July to September) is smaller than that in other seasons. This shows that the balance between factors that determine xCO_2s varies seasonally.

The slope of linear regression between SST and xCO_2s gets steeper in the region where SST < 5 °C because CO_2-rich water is supplied from deeper waters by the western subarctic circulation and vertical mixing.

In the Oyashio region and the region where SST < 16 °C, xCO_2s is very low and there is no clear relationship between SST and xCO_2s because phytoplankton blooms consume most of the CO_2 (green oval in Fig. 3a).

Based on these observations, we divided the subarctic region into three smaller regions: the northern subtropical region (SST ≥ 16 °C; Region C), the southern subarctic region (5 °C ≤ SST < 16 °C;

Region B) and the northern subarctic region (SST < 5 °C; Region A). We produced regression equations for each sub-region. Two equations are needed for the southern subarctic region to account for seasonal differences between summer and other seasons. The equation for Region A (SST < 5 °C) is as follows:

$$x\mathrm{CO}_2\mathrm{s} = 288.62 - 14.21 \cdot T_{10} + 1.40 \cdot Yr_{2000} \quad (\pm 24.6) \qquad (7).$$

The equation for Region B (Oct–Jun; 5 °C ≤ SST < 16 °C) is as follows:

$$x\mathrm{CO}_2\mathrm{s} = 345.42 - 3.10 \cdot T_{10} + 1.40 \cdot Yr_{2000} \quad (\pm 15.1) \qquad (8),$$

and for Jul–Sep (5 °C ≤ SST < 16 °C) as follows:

$$x\mathrm{CO}_2\mathrm{s} = 358.73 - 1.85 \cdot T_{10} + 1.40 \cdot Yr_{2000} \quad (\pm 21.2) \qquad (9).$$

For Region C (SST ≥ 16 °C), the equation is as follows:

$$x\mathrm{CO}_2\mathrm{s} = 248.10 + 9.86 \cdot T_{10} - 12.78 \cdot S_{33} + 0.76 \cdot Lon_{160} + 1.40 \cdot Yr_{2000} \quad (\pm 15.1) \qquad (10),$$

where T_{10}, S_{33}, Lon_{160} and Yr_{2000} are defined as [SST − 10], [SSS − 33], [longitude (°E) − 160] and [year − 2000], respectively.

It is also necessary to consider the biological activity in the regions off the Sanriku coast in Japan and around the Aleutian Islands (Ono et al., 2004; Sarma et al., 2006; Chierici et al., 2009). Chierici et al. (2009) reported that the use of log-transformed Chl-*a* data significantly improves the fit of the multiple regressions for estimating $p\mathrm{CO}_2$s.

We compared the logarithm of Chl-*a* with the residual error between estimated and observed $x\mathrm{CO}_2$s (Fig. 4a–4c) and found negative linear relationships. We generated linear regression equations to estimate the biological consumption of CO_2 (*Bio*) in each region.

Region A (SST < 5 °C): $Bio = -55.11 - 48.47 \cdot \ln[\mathrm{Chl\text{-}a}]$ (± 50.3) (11)

Region B (Oct–Jun ; 5 °C ≤ SST < 16 °C): $Bio = -44.85 - 36.27 \cdot \ln[\mathrm{Chl\text{-}a}]$ (± 29.3) (12)

Region B (Jul–Sep ; 5 °C ≤ SST < 16 °C): $Bio = -42.99 - 30.34 \cdot \ln[\mathrm{Chl\text{-}a}]$ (± 39.8) (13)

Negative values for *Bio* indicate that $x\mathrm{CO}_2$s is overestimated using SST and SSS and that CO_2 is consumed by biological activity. For the regions west of 160°E or north of 50°N only, where there is high biological activity, if Eq. 11–13 yield negative values for *Bio*, then the value for *Bio* is respectively added to $x\mathrm{CO}_2$s as estimated by Eq. 7–9. The introduction of the *Bio* term reduces the average bias of the estimates to ±10 ppm.

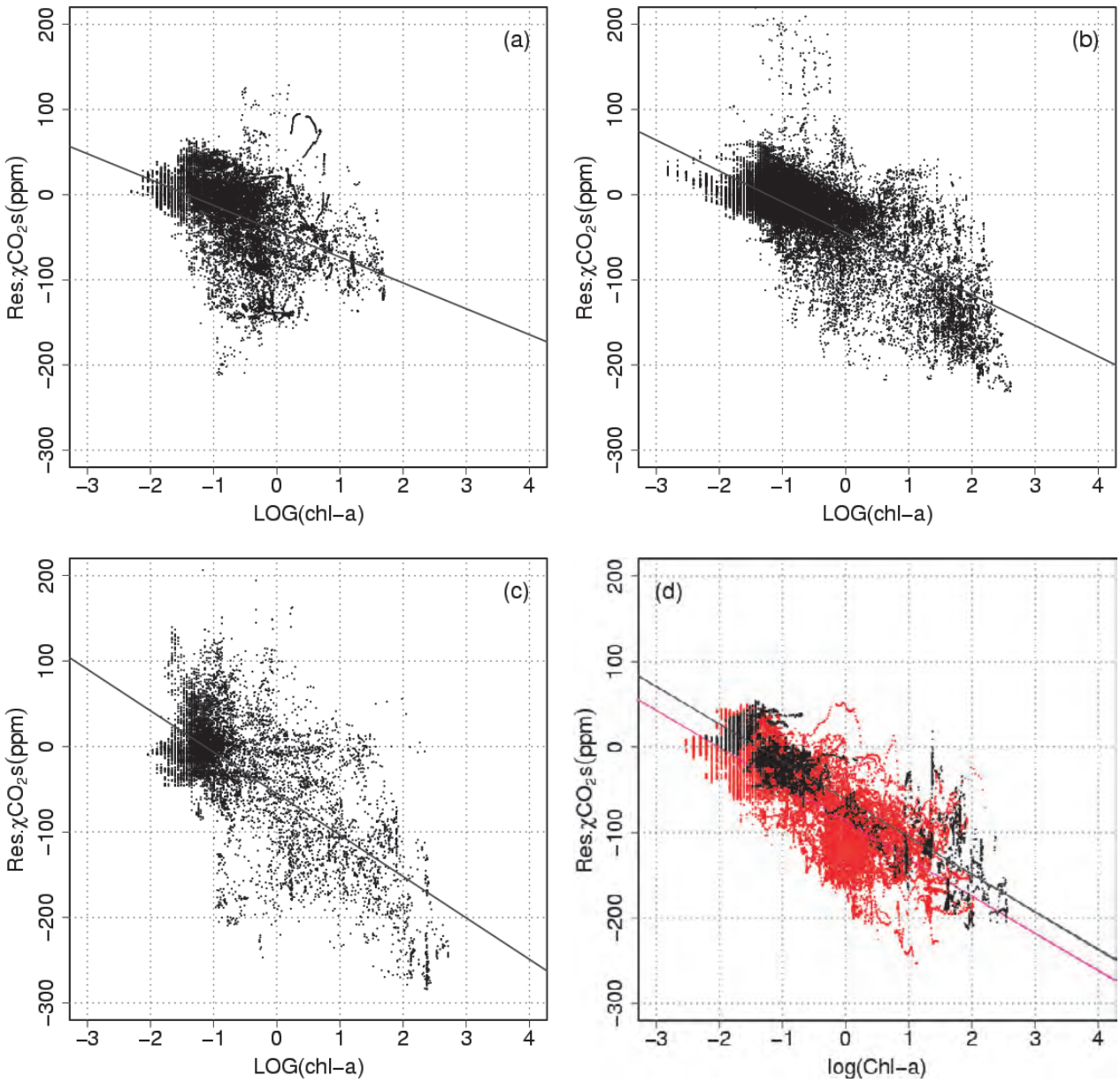

Figure 4. Relationships between the residual error between estimated and observed xCO_2s and the logarithm of chlorophyll-*a* concentrations determined by remote sensing from satellite. (a) The southern subarctic region within NP/A (summer: July–September), (b) the southern subarctic region within NP/A (winter: October–June), (c) the northern subarctic region within NP/A, (d) SST < 3℃ region within SP/A (black, October–December; red, January–April). Lines and shade areas are regression lines and 95% confidence intervals, respectively.

3.2.3.b. The South Pacific (SP/A)

The relationship between SST and xCO_2s changes at SST = 16 °C in the western portion of the South Pacific (140°E) and at SST = 10 °C in the east (70°W). This relationship is negative in the region of lower SSTs (orange oval in Fig. 3e) and positive at higher SSTs (red oval in Fig. 3e). In the region where SST < 3 °C, there is substantial biological consumption and no evident relationship between SST and xCO_2s when sea-ice melts in austral summer (green oval in Fig. 3e).

We divided the subantarctic South Pacific into three smaller regions using the following criteria:

1. Because the rates of increase of $x\mathrm{CO_2}$s differ between the northern region (north of 55°S) and the southern region (south of 55°S), as discussed in Section 3.1, the subantarctic South Pacific is divided into two regions at 55°S.
2. The northern region is divided into two regions by a boundary SST ($\mathrm{SST_{bnd}}$), defined as follows:

$$SST_{bnd} = 16 - \frac{6}{150}(longitude(°\mathrm{E}) - 140°\mathrm{E}) \qquad (14)$$

   The part of the northern region where SST < SST_{bnd} is called the northern subantarctic region (M) and where SST ≥ SST_{bnd} is the southern subtropical region (L).
3. The southern region (south of 55°S) is called the southern subantarctic region (N).

The relationship between SSS and n-$x\mathrm{CO_2}$s is negative in the southern subtropical region. We produced multiple regressions Eq. 15–17 to calculate $x\mathrm{CO_2}$s in the three regions using SST and SSS. For Region L (north of 55°S and SST ≥ $\mathrm{SST_{bnd}}$), the equation is as follows:

$$x\mathrm{CO_2s} = 322.90 + 2.23 \cdot T - 10.24 \cdot S_{33} + 0.44 \cdot Lon_{180} + 1.30 \cdot Yr_{2000} \quad (\pm 14.3) \qquad (15),$$

for Region M (north of 55°S and SST < $\mathrm{SST_{bnd}}$):

$$x\mathrm{CO_2s} = 399.97 - 6.62 \cdot T + 11.50 \cdot S_{33} + 1.30 \cdot Yr_{2000} \quad (\pm 15.0) \qquad (16),$$

and for Region N (south of 55°S):

$$x\mathrm{CO_2s} = 363.06 - 0.44 \cdot T + 4.19 \cdot S_{33} + 2.20 \cdot Yr_{2000} \quad (\pm 13.5) \qquad (17),$$

where Lon_{180} is the longitude (°E) minus 180.

In the Antarctic region (SST < 3°C), we introduce the *Bio* term to express biological consumption as in the subarctic region in the North Pacific. We produced two linear regression equations because the intercept of the regression between the logarithm of Chl-*a* concentration and the residual error of $x\mathrm{CO_2}$s from Eq. 17 changes between spring/early summer (October–December; black symbols in Fig. 4d) and late summer/autumn (January–April; red symbols in Fig. 4d). In areas where *Bio* was negative, as estimated by Eq. 18 and 19, it was added to $x\mathrm{CO_2}$s:

$$\text{Region N (Oct–Dec)}, \quad Bio = -61.05 - 43.94 \cdot \ln[\mathrm{Chl\text{-}a}] \quad (\pm 23.8) \qquad (18)$$

$$\text{Region N (Jan–Apr)}, \quad Bio = -87.56 - 43.49 \cdot \ln[\mathrm{Chl\text{-}a}] \quad (\pm 32.0) \qquad (19)$$

4. pCO_2s estimation and associated error

We estimated monthly pCO_2s in a 1° × 1° grid from 1985 through 2009 by using the grid data described in Section 2 and the empirical equations introduced in Section 3. Data for Chl-*a* by remote sensing have been available only since 1998. For pCO_2s estimates before 1998 we used the climatological Chl-*a*, which is the average of monthly remote sensing data sets from 1998 through 2009.

We generated time series of monthly pCO_2s and pCO_2a averaged in the five regions since 1985 (Fig. 5). The estimates for 25 years agree with observations very well in the five regions. For example, our method adequately reproduced the drastic decrease in pCO_2s in the equatorial region during 1997/1998 El Niño. The method also estimates pCO_2s in subarctic regions where large seasonal variations in pCO_2s occur because of biological consumption and vertical mixing.

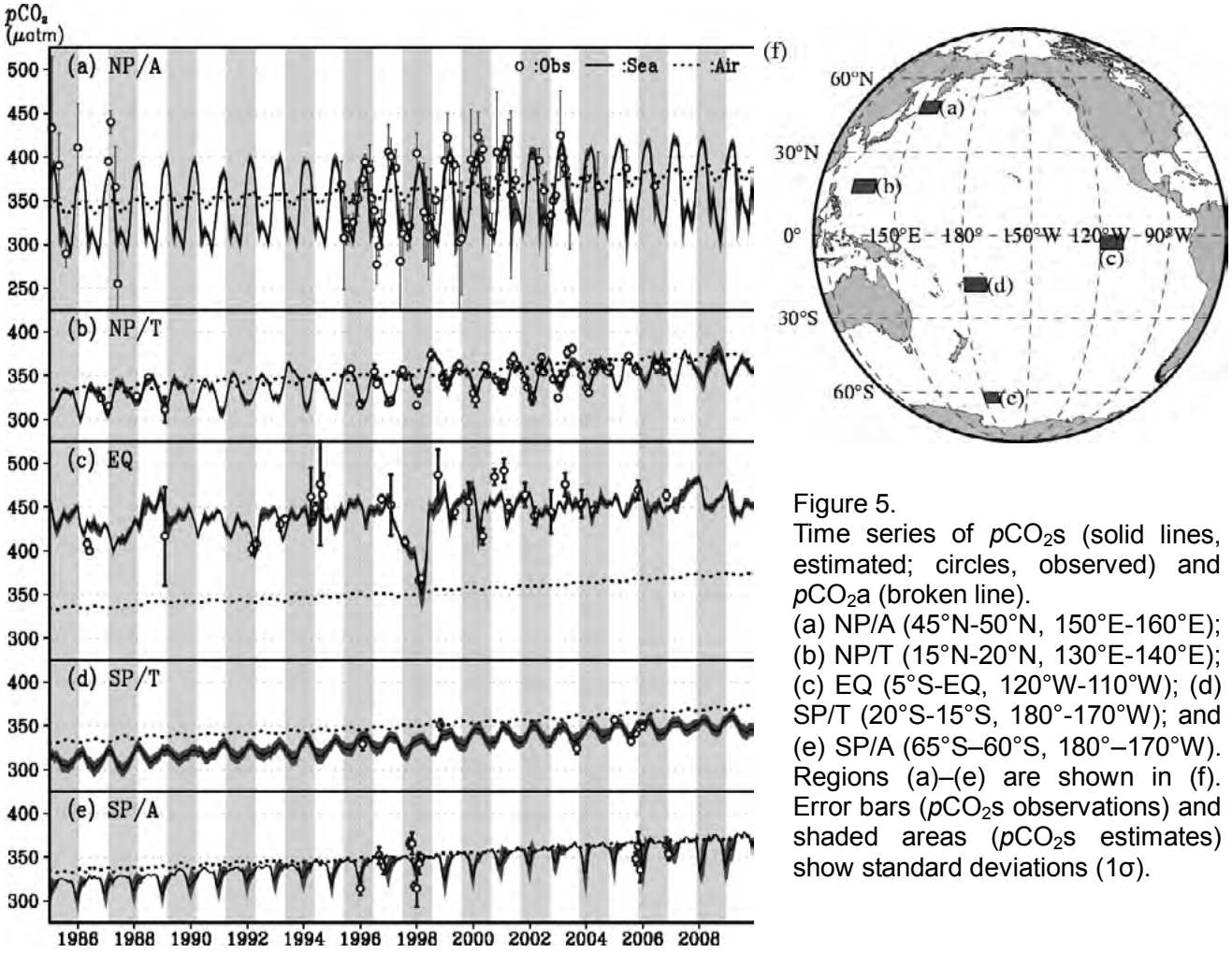

Figure 5.
Time series of pCO_2s (solid lines, estimated; circles, observed) and pCO_2a (broken line).
(a) NP/A (45°N-50°N, 150°E-160°E); (b) NP/T (15°N-20°N, 130°E-140°E); (c) EQ (5°S-EQ, 120°W-110°W); (d) SP/T (20°S-15°S, 180°-170°W); and (e) SP/A (65°S–60°S, 180°–170°W). Regions (a)–(e) are shown in (f). Error bars (pCO_2s observations) and shaded areas (pCO_2s estimates) show standard deviations (1σ).

We determined the annual mean bias and RMSE between pCO_2s estimates and observations in each region over 25 years. For error estimation in 2007 and 2008, we also used the latest LDEO Database V2008 (Takahashi et al., 2009a). The mean biases in all regions are small, ranging from −10 to +10 μatm (Fig. 6). The RMSE in the subarctic regions and the equatorial region (approximately 30 μatm) is relatively larger than that in the subtropical regions (about 20 μatm).

We used monthly mean SST, SSS and Chl-*a* data to estimate monthly pCO_2s fields. These data sets represent a different time-scale than observational data, which are instantaneous values. This difference in

time-scale causes some error in pCO_2s estimation.

The differences between estimates and observations in the subtropical and warm-pool regions are smaller than those in the equatorial upwelling region and subarctic regions. This is because the estimation errors in subtropical and equatorial warm-pool regions, where pCO_2s varies mainly because of the thermodynamic effect, are based almost entirely on SST data errors.

In the equatorial region, the boundaries between the upwelling region, the low salinity region and the warm-pool region are determined by monthly SSS data, but these boundaries actually shift over shorter time scales. This time lag in region division increases the estimation error in the equatorial region.

In the subpolar regions, monthly Chl-*a* fields are used for pCO_2s estimation. pCO_2s is very sensitive to Chl-*a* levels, which vary widely over short time intervals. Furthermore, climatological Chl-*a* was used for pCO_2s estimates before 1998. These factors increase RMSEs in the subpolar regions.

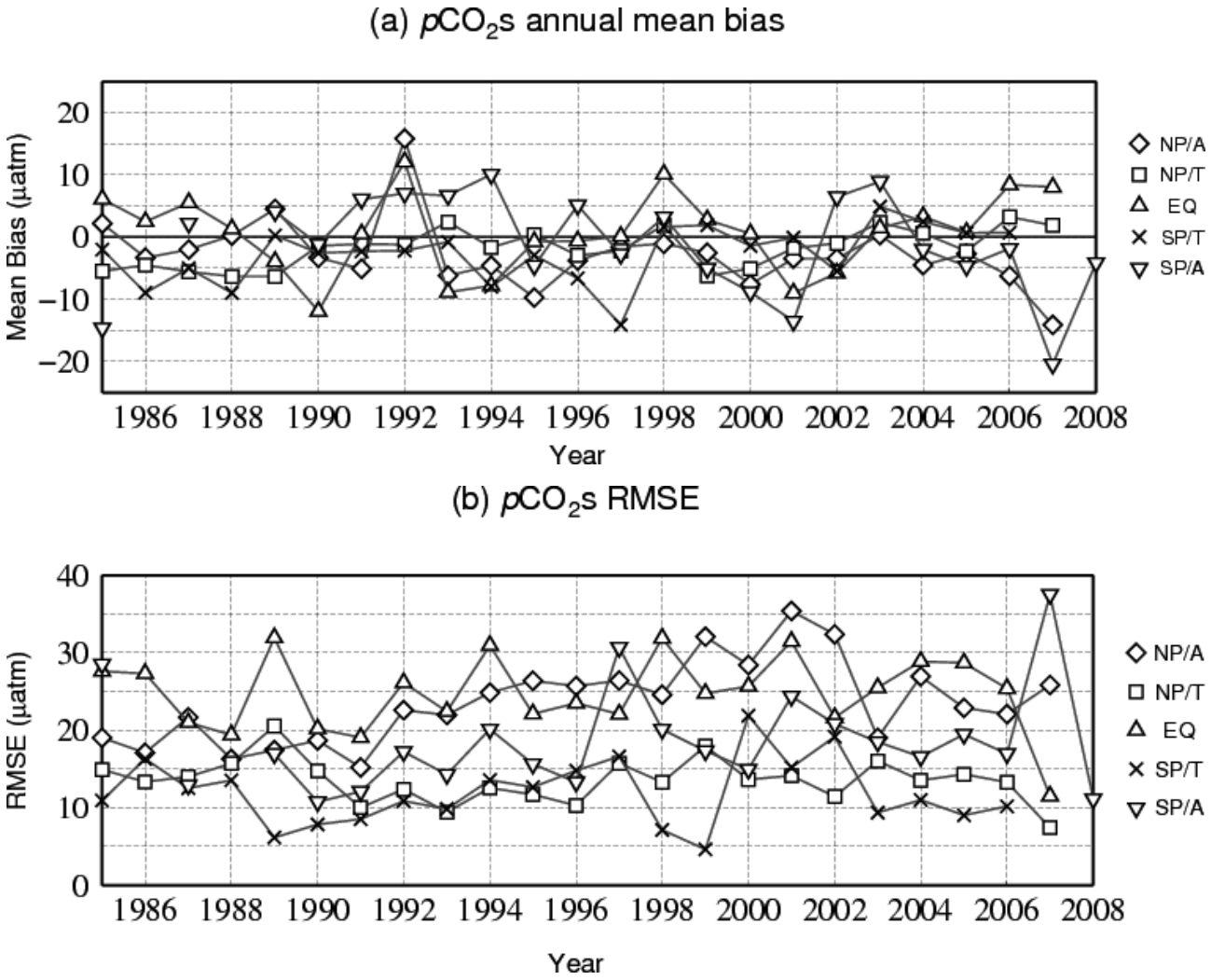

Figure 6. Annual mean biases (a) and annual RMSE (root mean square error) (b) between estimated and observed pCO_2s in each region. Bias is defined as $\Sigma(pCO_2\text{s [estimated]} - pCO_2\text{s [observed]})/n$, and RMSE is defined as $\sqrt{\Sigma(pCO_2\text{s [estimated]} - pCO_2\text{s [observed]})^2/(n-1)}$. n is the number of data.

5. Net sea-air CO_2 flux estimation

5.1. Computational method for estimating CO_2 flux

The net sea-air CO_2 flux (F_{CO_2}) can be estimated using Eq. 18:

$$F_{CO_2} = K \cdot \Delta pCO_2 \tag{18}$$

In this equation, K is the gas transfer coefficient and ΔpCO_2 is the difference in pCO_2 between sea and air (=pCO_2s − pCO_2a). K is the product of the gas transfer velocity (k) and the solubility of CO_2 in seawater (L). k is calculated by the method of Wanninkhof (1992), which uses monthly U_{10} values. L is based on the equation of Weiss (1974).

5.2. Seasonal average and variation of CO_2 flux

The 25-year mean monthly CO_2 flux maps for February, May, August and November show the typical horizontal distribution of the CO_2 flux from 1985 to 2009 (Fig. 7). In the equatorial region, pCO_2s is larger than pCO_2a throughout the year, and this region is a major CO_2 source for the atmosphere. This is because of the inorganic carbon supplied from the deeper oceanic layers through equatorial upwelling.

In the subtropical region, because biological CO_2 consumption is low and the mixed layer is shallow, pCO_2s varies with SST because of the thermodynamic effect. pCO_2s is therefore the highest when SST is the highest during summer in each hemisphere and CO_2 uptake in summer is less than in winter. In the North Pacific, pCO_2s in the western region and the coastal region off California is higher than in the other regions. The western region is affected by the Kuroshio and the coastal region off California is influenced by subarctic seawater rich in carbon. The region east of Hawaii is located in the marginal zone between subtropical warm water and subarctic cold water rich in carbon and nutrients; the subtropical water is cooled by the subarctic water and carbon is consumed through biological activity. As a result, pCO_2s in this region is relatively low. However, pCO_2s increases from west to east in the South Pacific. The coastal region off Peru in particular is influenced by coastal upwelling and emits CO_2 to the atmosphere.

In the subpolar regions, pCO_2s is the highest in winter because vertical mixing supplies carbon-rich water from lower layers. In the region east of Japan and in the antarctic region, pCO_2s decreases from spring to summer when phytoplankton consumes CO_2.

The marginal zone between the subtropical and subarctic regions in the Pacific is a major CO_2 sink. Because SST decreases and seasonal wind intensifies in winter, pCO_2s decreases from the thermodynamic effect and the gas transfer coefficient increases. As a result, CO_2 uptake is highest in winter.

Larger standard deviations of CO_2 flux are seen around the equatorial region and the boundary between the subtropical and subpolar regions (Fig. 8). pCO_2s in the equatorial region is affected by ENSO, as mentioned in Section 4. The ENSO cycle affects pCO_2s and wind patterns, causing variations in the CO_2 flux. In the North Pacific boundary region, SST and SLP variations caused by the PDO are predominant. The PDO could affect pCO_2s or U_{10} (and the gas transfer velocity) through anomalies in SST and SLP.

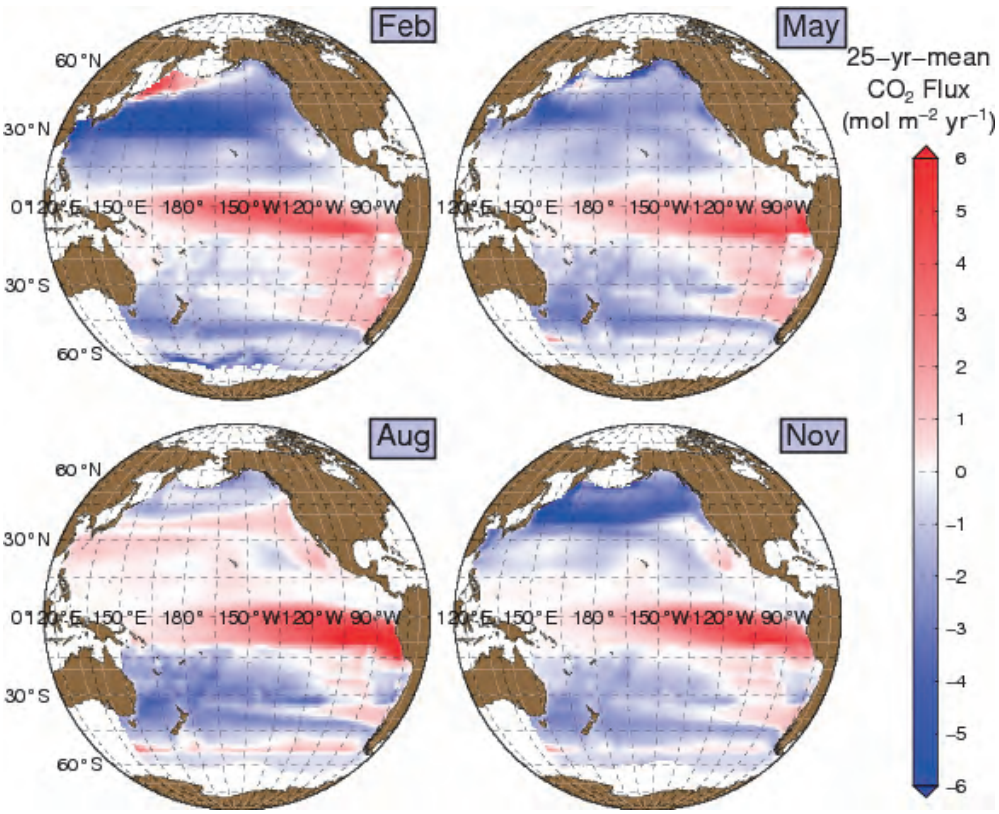

Figure 7. Monthly mean CO_2 flux maps for February, May, August and November. The color scale shows the level of CO_2 source or sink.

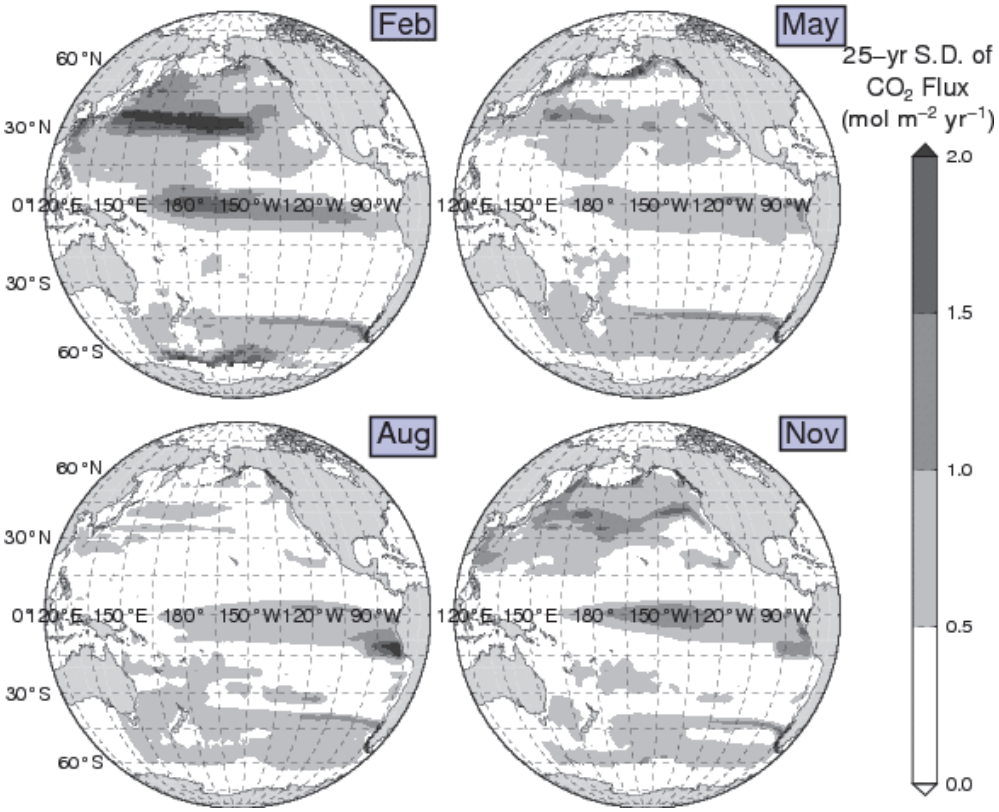

Figure 8. Standard deviations of monthly CO_2 flux (mol m^{-2} yr^{-1}) in February, May, August and November.

5.3. Time series of area-integrated CO_2 flux

We calculated the area-integrated monthly and annual CO_2 flux from 1985 through 2009 (Fig. 9). In the equatorial region, CO_2 outgassing varies with ENSO. CO_2 emission decreases during El Niño periods (ENSO warm phase) and increases for La Niña periods (ENSO cold phase). For the 1997/1998 El Niño period in particular, CO_2 emission was 70% of that during normal periods.

In contrast, seasonal variation predominates in the subtropical regions, and CO_2 uptake decreases in summer and increases in winter. The amplitude of the variation in CO_2 flux is greater in the northern hemisphere than in the southern. This reflects the larger seasonal SST amplitude and more severe winter winds in the northern hemisphere.

As in the subtropical regions, there is seasonal variation in the subarctic region as well. Unlike the subtropical regions, the CO_2 flux in the subarctic region is at a minimum in spring due to biological uptake of CO_2. There is seasonal variation in CO_2 flux in the subantarctic region, with a maximum uptake by the sea in austral summer and a minimum uptake in austral winter. This is because the amount of inorganic carbon supplied by vertical mixing is small and biological uptake increases in austral summer.

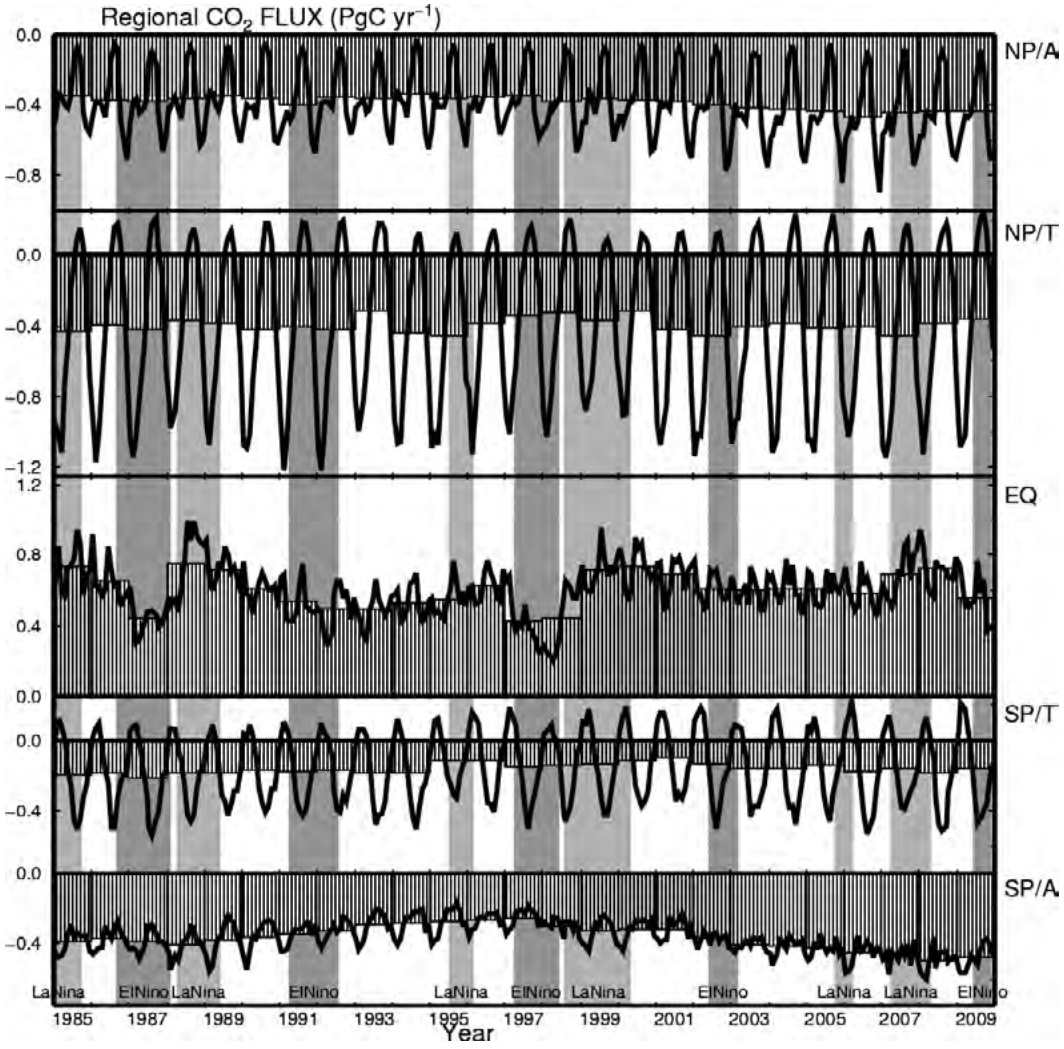

Figure 9. Time series of regional CO_2 flux (PgC yr^{-1}) for the Pacific Ocean. Lines and boxes show monthly and annual CO_2 flux, respectively. Shading indicates ENSO events: dark grey, El-Niño; light grey, La-Niña.

5.4. Comparison with the climatological CO_2 flux

We compared the meridional distribution of the CO_2 flux in 2000 determined in this study with the climatological CO_2 flux for the reference year 2000 as reported by Takahashi et al. (2009b) (Fig. 10). The results of this study correspond qualitatively with the climatology. However in the equatorial region the flux estimated in this study is double the climatological flux estimate.

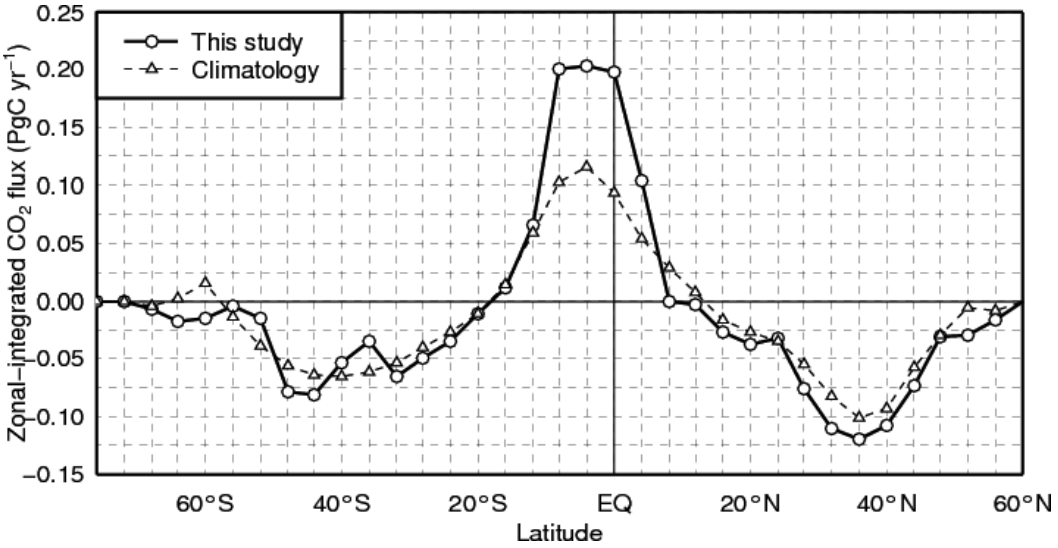

Figure 10. Meridional distribution of the zonally-integrated CO_2 flux (PgC yr^{-1}) in 2000 from this study (solid line) and the climatological CO_2 flux in the reference year 2000 from Takahashi et al. (2009b) (dashed line).

Table 3 presents the comparison between the flux determined in this study and the climatological flux estimate in each zonal band. The absolute values from this study are larger than those of the climatology in all zonal bands. In this study we used different U_{10} analysis data and a different equation for the gas transfer coefficient than used for the climatology data. As a result, the gas transfer coefficients in this study are from about 1.5 to 2 times those of the climatology.

Table 3. Comparison between the CO_2 fluxes estimated in this study and the climatological CO_2 flux in each zonal band. The gas transfer coefficient used in this study is from the equation of Wanninkhof (1992). Positive and negative CO_2 fluxes refer to sea-to-air or air-to-sea transfers of CO_2, respectively. The column "The average values for 1985–2009" is the average and standard deviation of the annual mean CO_2 fluxes between 1985 and 2009.

Zone	This study		Takahashi *et al*. (2009b)
	In 2000 (PgC yr^{-1})	Average 1985-2009 (PgC yr^{-1})	(PgC yr^{-1})
N. of 50°N	–0.06	–0.06±0.01	–0.03
14°N-50°N	–0.64	–0.70±0.05	–0.50
14°S-14°N	+0.77	+0.62±0.10	+0.48
50°S-14°S	–0.42	–0.46±0.08	–0.41
Sum.	–0.34	–0.59±0.14	–0.46

Because a La Niña event continued until the spring of 2000, the pCO_2s values in this study, which reflect the real-time oceanic conditions, are larger than the climatological pCO_2s in the equatorial region (Fig. 11). The difference between the CO_2 flux estimates results from the difference in gas transfer coefficient and

the La Niña event.

In the Pacific north of 50°S, the mean flux from 1985 through 2009 estimated in this study is −0.59 PgC yr^{-1}; the flux estimate for 2000 is −0.34 PgC yr^{-1} and the climatological flux in the reference year 2000 is −0.46 PgC yr^{-1}. The estimated annual CO_2 flux in 2000 from this study is smaller uptake than the climatological estimate because of the influence of La Niña. The mean annual flux from this study is larger uptake than the climatological flux estimate because of the difference in the gas transfer coefficients.

The surface of the Pacific Ocean accounts about 46% of the ocean surface worldwide. However, the average CO_2 uptake in the Pacific as estimated in this study is about 32% of the total absorption by the Global Ocean (2.2 PgC yr^{-1}; IPCC, 2007). The proportional CO_2 uptake in the Pacific Ocean is smaller than the proportional area because of the Pacific equatorial region, which is the area of greatest CO_2 release in the world.

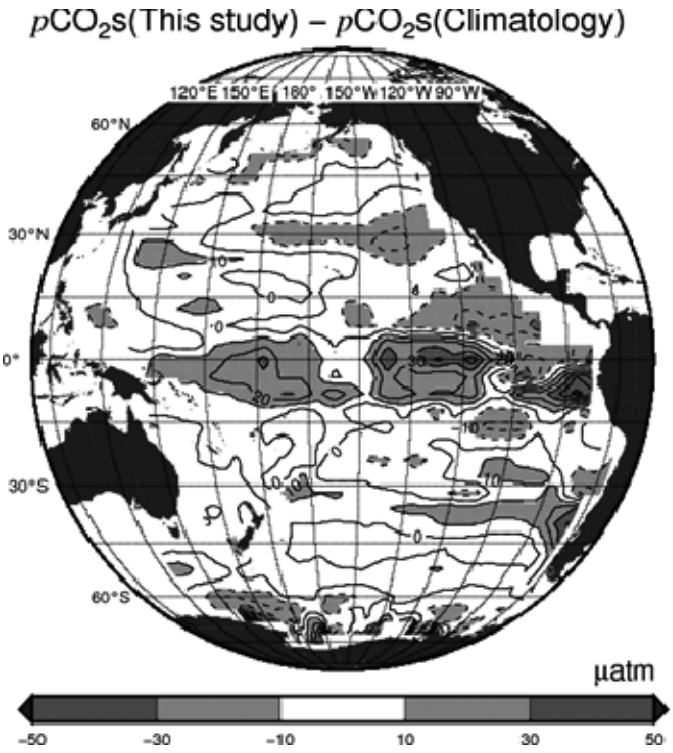

Figure 11. Mean difference between the pCO_2s values in 2000 estimated in this study and the climatological pCO_2s values (Takahashi et al., 2009b). The difference is defined as the value from this study minus the climatological value.

5.5. Effects of gas transfer coefficient equations on CO_2 flux

We used the formula of Wanninkhof (1992; hereafter "W92") to estimate CO_2 flux. In other recent studies, other formulas have been proposed, such as those of Nightingale et al. (2000; hereafter "N00") and Sweeney et al. (2007; hereafter "S07"). We compared the CO_2 fluxes estimated using gas transfer coefficients calculated using these three formulas. The results of this comparison are summarized in Table 4. Absolute value of annual mean CO_2 flux estimates based on N00 using JRA25/JCDAS wind speed fields were the lowest and those using W92 were the highest. In each region, the difference between gas transfer coefficients is 15–20%. This difference is comparable to the uncertainty in the gas transfer coefficients of about 30% (Sweeney et al., 2007).

5.6. Effect of wind speed on CO_2 flux

To calculate gas transfer coefficients we used not only the wind velocity fields from JRA25/JCDAS but also those from National Centers for Environmental Prediction / National Center for Atmospheric Research (NCEP/NCAR) Reanalysis I (Kalnay et al., 1996; hereinafter CDAS1) and from a

cross-calibrated, multi-platform (CCMP), multi-instrument ocean surface wind velocity data set (Ardizzone et al., 2009). We used SLP fields from JRA25/JCDAS because the mean SLP difference between JRA25/JCDAS and CDAS1 is about 1 hPa and this results in a difference in pCO_2s of only 0.1% (0.4 μatm). The effect of the SLP difference is less than the pCO_2s estimation error of −10 to +10 μatm.

In Table 4, we summarize the annual regional CO_2 flux as estimated using three different types of U_{10} data. Except for the equatorial region (14°S–14°N), the CO_2 flux estimates agree with each other. In the equatorial region, CO_2 emission based on CDAS1 is the smallest among the three wind velocity fields. For example, the difference in CO_2 flux estimates based on the JRA25/JCDAS and CDAS1 U_{10} fields using the W92 equation is about 20% (0.12 PgC yr^{-1}). This is because the U_{10} of CDAS1 is 10% weaker than that of JRA25/JCDAS due to the differences of models and assimilated datasets. When the gap between U_{10} values is 10%, that between gas transfer coefficients accounts for about 20% of the difference because the gas transfer coefficient is proportional to the square of U_{10}. For the entire Pacific Ocean, estimates using JRA25/JCDAS show lower CO_2 uptake than those using CDAS1 because of higher CO_2 emission in the equatorial region.

Table 4. Comparison of different estimates of the CO_2 flux (PgC yr^{-1}) for each zonal band using equations for gas transfer coefficients from three sources — Wanninkhof (1992; W92), Nightingale et al. (2000; N00) and Sweeney et al. (2007; S07) — and U_{10} fields from JRA25/JCDAS, NCEP/NCAR Reanalysis I, and a cross-calibrated, multi-platform (CCMP) dataset. Values for CO_2 flux are means and standard deviations from 1985 through 2009 (1990–2009 for CCMP).

	Gas transfer velocity	JRA25/JCDAS	CDAS1	CCMP	Clim
N. of 50N	W92	-0.06 ± 0.01	-0.07 ± 0.01	-0.06 ± 0.01	
	N00	-0.05 ± 0.01	-0.05 ± 0.01	-0.05 ± 0.01	*-0.03*
	S07	-0.05 ± 0.01	-0.06 ± 0.01	-0.05 ± 0.01	
14N-50N	W92	-0.70 ± 0.05	-0.70 ± 0.04	-0.75 ± 0.05	
	N00	-0.51 ± 0.03	-0.51 ± 0.03	-0.53 ± 0.03	*-0.50*
	S07	-0.56 ± 0.03	-0.56 ± 0.03	-0.55 ± 0.03	
14S-14N	W92	0.62 ± 0.10	0.50 ± 0.07	0.68 ± 0.09	
	N00	0.44 ± 0.06	0.37 ± 0.05	0.48 ± 0.06	*0.48*
	S07	0.45 ± 0.07	0.37 ± 0.05	0.46 ± 0.06	
50S-14S	W92	-0.46 ± 0.08	-0.48 ± 0.07	-0.52 ± 0.07	
	N00	-0.34 ± 0.05	-0.35 ± 0.05	-0.37 ± 0.05	*-0.41*
	S07	-0.37 ± 0.06	-0.38 ± 0.05	-0.39 ± 0.05	
S. of 50S	W92	-0.11 ± 0.04	-0.10 ± 0.03	-0.09 ± 0.02	
	N00	-0.08 ± 0.03	-0.07 ± 0.03	-0.06 ± 0.02	-
	S07	-0.09 ± 0.04	-0.08 ± 0.03	-0.07 ± 0.02	
Pacific	W92	-0.70 ± 0.14	-0.84 ± 0.11	-0.74 ± 0.14	
	N00	-0.53 ± 0.10	-0.62 ± 0.08	-0.54 ± 0.10	-
	S07	-0.62 ± 0.10	-0.71 ± 0.09	-0.59 ± 0.10	

6. Summary and conclusions

We developed an empirical method to estimate monthly pCO_2s and sea-air CO_2 flux over the Pacific since 1985 using the LDEO database V1.0 (Takahashi et al., 2008) of global pCO_2s observations. First, we determined the long-term trend of pCO_2s. Second, we analyzed regional and seasonal variations of pCO_2s. We divided the Pacific Ocean into 14 regions and derived multiple regression equations for estimating monthly pCO_2s for each region incorporating data for SST, SSS and Chl-*a*. Previously it had been difficult to reproduce pCO_2s in the subpolar regions where there are spring blooms and high net biological consumption of inorganic carbon, but the bias in the estimates was significantly reduced by including Chl-*a* data in the analysis. Mean bias of estimated pCO_2s in each region ranged from –10 to +10 μatm.

The estimated mean annual CO_2 flux in the Pacific Ocean is -0.70 ± 0.14 PgC yr^{-1} (negative value indicates uptake by the ocean) for the period from 1985 to 2009. The CO_2 flux varies seasonally and inter-annually. While there is CO_2 emission throughout the year in the equatorial region, there is strong CO_2 uptake along the mid-latitudes in winter. We found that CO_2 flux in the equatorial region varies largely with ENSO. In particular, the CO_2 emission decreased by 0.2 PgC yr^{-1} during the 1997/1998 El Nino event. The region included in this study is about 46% of the global ocean. To further understand the global carbon cycle, it will be necessary to investigate whether the empirical method developed in this study can be applied to the Atlantic and Indian oceans to expand the region of CO_2 flux estimation.

There is a significant uncertainty remaining in the CO_2 flux estimates. The different gas transfer coefficient equations used in this study resulted in differences of 15% to 20% in estimated fluxes. The CO_2 emission in the equatorial region, when evaluated using the wind-speed product from the JRA25/JCDAS reanalysis, is about 0.12 PgC yr^{-1} (20%) higher than that estimated using CDAS1. The CO_2 flux estimates in the other regions are consistent between reanalysis data sets.

To reduce the uncertainty in CO_2 flux estimates, it will be necessary to continue investigations into better wind-speed analysis and gas transfer coefficients. There are plans to update the global pCO_2s database annually with the accumulated pCO_2s observation data. Therefore, there should be a continuous review of the equations and the regional divisions used for pCO_2s estimation to reduce uncertainties where the data are sparse. It is important to use observations to monitor inter-annual variations and long-term trends of pCO_2s.

Furthermore, it is important to compare CO_2 flux as estimated using other approaches such as atmospheric CO_2 inversion, forward ocean carbon cycle modeling, and ocean carbon inversion. Discrepancies in the estimates from these methods must be reduced to better understand the carbon cycle and to improve projections of global warming.

Acknowledgments

We are deeply grateful to Dr. Taro Takahashi and his colleagues for having pioneered the measurement of surface water pCO_2 and for synthesizing large numbers of data from throughout the oceans. We thank the other original measurement teams and their support staffs for having struggled to collect data from individual cruises; none of the synthesis efforts for the database would have been possible without their hard work. We also thank members of the Global Environment and Marine Department of the Japan Meteorological Agency and the Geochemical Research Department of the Meteorological Research Institute for providing support for this work.

References

Antonov, J. I., D. Seidov, T. P. Boyer, R. A. Locarnini, A. V. Mishonov, H. E. Garcia, O. K. Baranova, M. M. Zweng, and D. R. Johnson (2010): World Ocean Atlas 2009, Volume 2: Salinity. S. Levitus, Ed. NOAA Atlas NESDIS 69, U.S. Government Printing Office, Washington, D.C., 184 pp.

Ardizzone, J., R. Atlas, R. N. Hoffman, J. C. Jusem, S. M. Leidner, and D. F. Moroni (2009): New multiplatform ocean surface wind product available. EOS Trans. 90, 231.

Chierici, M., A. Olsen, T. Johannessen, J. Triñanes, and R. Wanninkhof (2009): Algorithms to estimate the carbon dioxide uptake in the northern North Atlantic using shipboard observations, satellite and ocean analysis data. Deep-Sea Res. II, 56, 630-639, doi:10.1016/j.dsr2.2008.12.014

Cosca, C. E., R. A. Feely, J. Boutin, J. Etcheto, M. J. McPhaden, F. P. Chavez, and P. G. Strutton (2003): Seasonal and interannual CO_2 fluxes for the central and eastern equatorial Pacific Ocean as determined from fCO_2-SST relationships. J. Geophys. Res., 108(C8), 3278, doi:10.1029/2000JC000677

Feely, R. A., T. Takahashi, R. Wanninkhof, M. J. McPhaden, C. E. Cosca, S. C. Sutherland, and M.-E. Carr (2006): Decadal variability of the air-sea CO_2 fluxes in the equatorial Pacific Ocean. J. Geophys. Res., 111, C08S90, doi:10.1029/2005JC003129.

Feldman, G. C. and C. R. McClain (2010a): Ocean Color Web, SeaWiFS Reprocessing 2009.1, NASA Goddard Space Flight Center. Eds. Kuring, N., Bailey, S. W. May 2010. http://oceancolor.gsfc.nasa.gov/

Feldman, G. C. and C. R. McClain (2010b): Ocean Color Web, MODIS-Aqua Reprocessing 2009.1, NASA Goddard Space Flight Center. Eds. Kuring, N., Bailey, S. W. May 2010. http://oceancolor.gsfc.nasa.gov/

Friederich, G. E., J. Ledesma, O. Ulloa, and F. P. Chavez (2008): Air-sea carbon dioxide fluxes in the coastal southeastern tropical Pacific. Progress in Oceanography, 76, 156-166, doi:10.1016/j.pocean.2008.10.001.

Inoue H. Y. and M. Ishii (2005): Variations and trends of CO_2 in the surface seawater in the Southern Ocean south of Australia between 1969 and 2002. Tellus, 57B, 58-69.

Inoue, H.Y., M. Ishii, H. Matsueda, S. Saito, T. Midorikawa, and K. Nemoto (1999): MRI measurements of partial pressure of CO_2 in surface waters of the Pacific during 1968 to 1970: re-evaluation and comparison of data with those of the 1980s and 1990s. Tellus, 51B, 830-848.

[IPCC] Intergovernmental Panel on Climate Change (2007): Climate Change 2007: The Physical Science Basis. Working Group I Contribution to the Fourth Assessment Report of the IPCC. Cambridge University Press, Cambridge, UK and New York, NY, USA, 996 pp.

Ishii, M., H. Y. Inoue, T. Midorikawa, S. Saito, T. Tokieda, D. Sasano, A. Nakadate, K. Nemoto, N. Metzl, C. S. Wong, and R. A. Feely (2009): Spatial variability and decadal trend of the oceanic CO_2 in the western equatorial Pacific warm/fresh water. Deep-Sea Res. II, 56, 591-606, doi:10.1016/j.dsr2.2009.01.002.

Kalnay, E., M. Kanamitsu, R. Kistler, W. Collins, D. Deaven, L. Gandin, M. Iredell, S. Saha, G. White, J. Woollen, Y. Zhu, M. Chelliah, W. Ebisuzaki, M. Chelliah, W. Ebisuzaki, W. Higgins, J. Janowiak, K. C. Mo, C. Ropelewski, J. Wang, A. Leetmaa, R. Reynolds, R. Jenne, and D. Joseph (1996): The NCEP/NCAR 40-Year Reanalysis Project. Bull. Amer. Meteor. Soc., 77, 437-472.

Kurihara, Y., T. Sakurai, and T. Kuragano (2006): Global daily sea surface temperature analysis using data from satellite microwave radiometer, satellite infrared radiometer and in-situ observations. Sokko-jiho, 73, S1-S18 (in Japanese).

Locarnini, R. A., A. V. Mishonov, J. I. Antonov, T. P. Boyer, H. E. Garcia, O. K. Baranova, M. M. Zweng, and D. R. Johnson (2010): World Ocean Atlas 2009, Volume 1: Temperature. S. Levitus, Ed. NOAA Atlas NESDIS 68, U.S. Government Printing Office, Washington, D.C., 184 pp.

Maki, T., M. Ikegami., T. Fujita, T. Hirahara, K. Yamada, K. Mori, A. Takeuchi, Y. Tsutsumi, K. Suda, and T. J. Conway (2010): New technique to analyse global distributions of CO_2 concentrations and fluxes from non-processed observational data. Tellus, 62B, 797-809, doi:10.1111/j.1600-0889.2010.00488.x.

Murata, A., K. Fushimi, H. Yoshikawa, M. Hirota, K. Nemoto, M. Okabe, H. Yabuki, and I. Asanuma (1996): Evaluation of the CO_2 Exchange at Sea Surface in the Western North Pacific: Distributions of the ΔpCO_2 and the CO_2 Flux. J. Meteor. Res., 48, 2, 33-58.

Nakadate, A. and M. Ishii (2007): Estimation of the Sea-to-Air CO_2 Flux in the Equatorial Pacific. Sokko-jiho, 74, S163-S176 (in Japanese).

Nightingale, P. D., G. Malin, C. S. Law, A. J. Watson, P. S. Liss, M. I. Liddicoat, J. Boutin, and R. C. Upstill-Goddard (2000): In situ evaluation of air-sea gas exchange parameterizations using novel conservative and volatile tracers. Global Biogeochem. Cycles, 14, 373-387.

Ono, T., T. Saino, N. Kurita, and K. Sasaki (2004): Basin-scale extrapolation of shipboard pCO_2 data using satellite SST and Chla. Int. J. Remote Sens., 25, 3803- 3815.

Onogi, K., J. Tsutsui, H. Koide, M. Sakamoto, S. Kobayashi, H. Hatsushika, T. Matsumoto, N. Yamazaki, H. Kamahori, K. Takahashi, S. Kadokura, K. Wada, K. Kato, R. Oyama, T. Ose, N. Mannoji, and R. Taira (2007): The JRA-25 Reanalysis. J. Meteor. Soc. Japan, 85, 369-432.

Park, G. -H., K. Lee, R. Wanninkhof, and R. A. Feely (2006): Empirical temperature-based estimates of variability in the oceanic uptake of CO_2 over the past 2 decades. J. Geophys. Res., 111, C07S07, doi:10.1029/2005JC003090.

Park, G. -H., R. Wanninkhof, S. C. Doney, T. Takahashi, K. Lee, R. A. Feely, C. Sabine, J. Triñanes, and I. Lima (2010): Variability of global air-sea CO_2 fluxes over the last three decades. Tellus, 62B, doi: 10.1111/j.1600-0889.2010.00498.x, 352-368.

Sarma, V. V. S. S., T. Saino, K. Sasaoka, Y. Nojiri, T. Ono, M. Ishii, H. Y. Inoue, and K. Matsumoto (2006): Basin-scale pCO_2 distribution using satellite sea surface temperature, Chl *a*, and climatological salinity in the

North Pacific in spring and summer. Global Biogeochem. Cycles, 20, GB3005, doi:10.1029/2005GB002594

Sweeney, C., E. Gloor, A. R. Jacobson, R. M. Key, G. McKinley, J. L. Sarmiento, and R. Wanninkhof (2007): Constraining global air-sea gas exchange for CO_2 with recent bomb 14C measurements. Global Biogeochem. Cycles, 21, GB2015, doi:10.1029/2006GB002784.

Takahashi, T., J. Olafsson, J. Goddard, D. W. Chipman, and S. C. Sutherland (1993): Seasonal variation of CO_2 and nutrients in the high-latitude surface oceans: A comparative study. Global Biogeochem. Cycles 7, 843-878.

Takahashi, T., S. C. Sutherland, C. Sweeney, A. Poisson, N. Metzl, B. Tilbrook, N. Bates, R. Wanninkhof, R. A. Feely, C. Sabine, J. Olafsson, and Y. Nojiri (2002): Global sea-air CO_2 flux based on climatological surface ocean pCO_2, and seasonal biological and temperature effects. Deep-Sea Res. II, 49(9-10), 1601-1622.

Takahashi, T., S. C. Sutherland, and A. Kozyr (2008): Global Ocean Surface Water Partial Pressure of CO_2 Database: Measurements Performed during 1968-2006 (Version 1.0). ORNL/CDIAC-152, NDP-088, Carbon Dioxide Information Analysis Center, Oak Ridge National Laboratory, U. S. Department of Energy, Oak Ridge, TN, 20 pp.

Takahashi, T., S. C. Sutherland, and A. Kozyr (2009a): Global Ocean Surface Water Partial Pressure of CO_2 Database: Measurements Performed during 1968-2008 (Version 2008). ORNL/CDIAC-152, NDP-088(V2008), Carbon Dioxide Information Analysis Center, Oak Ridge National Laboratory, U. S. Department of Energy, Oak Ridge, TN, 20 pp.

Takahashi, T., S. C. Sutherland, R. Wanninkhof, C. Sweeney, R. A. Feely, D. W. Chipman, B. Hales, G. Friederich, F. Chavez, C. Sabine, A. Watson, D. C. E. Bakker, U. Schuster, N. Metzl, H. Yoshikawa-Inoue, M. Ishii, T. Midorikawa, Y. Nojiri, A. Kortzinger, T. Steinhoff, M. Hoppema, J. Olafsson, T. S. Arnarson, B. Tilbrook, T. Johannessen, A. Olsen, R. Bellerby, C. S. Wong, B. Delille, N. R. Bates, and H. J. W. de Baar (2009b): Climatological mean and decadal changes in surface ocean pCO_2, and net sea-air CO_2 flux over the global oceans. Deep-Sea Res. II, 56, 554-577.

Usui, N., S. Ishizaki, Y. Fujii, H. Tsujino, T. Yasuda, and M. Kamachi (2006): Meteorological Research Institute multivariate ocean variational estimation (MOVE) system: Some early results. Adv. Space Res., 37, 806-822.

Wanninkhof, R. (1992): Relationship between wind speed and gas exchange over the ocean. J. Geophys. Res., 97, 7373-7392.

Weiss, R. F. (1974): Carbon dioxide in water and seawater: the solubility of a nonideal gas. Mar. Chem., 2, 203-215.

Appendix

Table A1. Abbreviations

Abbreviation	Meaning
CO_2	Carbon dioxide
xCO_2s	CO_2 concentration in surface seawater (ppm)
pCO_2s	CO_2 partial pressure in surface seawater (μatm)
n-xCO_2s	xCO_2s normalized to 10 °C (ppm)
pCO_2a	CO_2 partial pressure in the air (μatm)
SST	Sea surface temperature (°C)
SSS	Sea surface salinity
SLP	Sea-level pressure (hPa)
U_{10}	Wind speed at 10 m above sea level
Chl-*a*	Concentration of chlorophyll-*a* (mg m^{-3})
ENSO	El Niño/Southern Oscillation
PDO	Pacific Decadal Oscillation
NP/A	Subarctic region of the North Pacific (35°N–60°N)
NP/T	Subtropical region of the North Pacific (6°N–34°N)
EQ	Equatorial region of the Pacific (10°S–5°N)
SP/T	Subtropical region of the South Pacific (34°S–11°S)
SP/A	Subantarctic region of the South Pacific (75°S–35°S)

気象研究所技術報告一覧表

第１号　バックグラウンド大気汚染の測定法の開発（地球規模大気汚染特別研究班，1978）
Development of Monitoring Techniques for Global Background Air Pollution. (MRI Special Research Group on Global Atmospheric Pollution, 1978)

第２号　主要活火山の地殻変動並びに地熱状態の調査研究（地震火山研究部，1979）
Investigation of Ground Movement and Geothermal State of Main Active Volcanoes in Japan. (Seismology and Volcanology Research Division, 1979)

第３号　筑波研究学園都市に新設された気象観測用鉄塔施設（花房龍男・藤谷徳之助・伴野　登・魚津　博，1979）
On the Meteorological Tower and Its Observational System at Tsukuba Science City. (T. Hanafusa, T. Fujitani, N. Banno, and H. Uozu, 1979)

第４号　海底地震常時観測システムの開発（地震火山研究部，1980）
Permanent Ocean－Bottom Seismograph Observation System. (Seismology and Volcanology Research Division, 1980)

第５号　本州南方海域水温図－400m（又は 500m）深と 1,000m 深－（1934－1943 年及び 1954－1980 年）（海洋研究部，1981）
Horizontal Distribution of Temperature in 400m (or 500m) and 1,000m Depth in Sea South of Honshu, Japan and Western －North Pacific Ocean from 1934 to 1943 and from 1954 to 1980. (Oceanographical Research Division, 1981)

第６号　成層圏オゾンの破壊につながる大気成分及び紫外日射の観測（高層物理研究部，1982）
Observations of the Atmospheric Constituents Related to the Stratospheric ozon Depletion and the Ultraviolet Radiation. (Upper Atmosphere Physics Research Division, 1982)

第７号　83 型強震計の開発（地震火山研究部，1983）
Strong－Motion Seismograph Model 83 for the Japan Meteorological Agency Network. (Seismology and Volcanology Research Division, 1983)

第８号　大気中における雪片の融解現象に関する研究（物理気象研究部，1984）
The Study of Melting of Snowflakes in the Atmosphere. (Physical Meteorology Research Division, 1984)

第９号　御前崎南方沖における海底水圧観測（地震火山研究部・海洋研究部，1984）
Bottom Pressure Observation South off Omaezaki, Central Honsyu. (Seismology and Volcanology Research Division and Oceanographical Research Division, 1984)

第 10 号　日本付近の低気圧の統計（予報研究部，1984）
Statistics on Cyclones around Japan. (Forecast Research Division, 1984)

第 11 号　局地風と大気汚染質の輸送に関する研究（応用気象研究部，1984）
Observations and Numerical Experiments on Local Circulation and Medium－Range Transport of Air Pollutions. (Applied Meteorology Research Division, 1984)

第 12 号　火山活動監視手法に関する研究（地震火山研究部，1984）
Investigation on the Techniques for Volcanic Activity Surveillance. (Seismology and Volcanology Research Division, 1984)

第 13 号　気象研究所大気大循環モデル－Ⅰ（MRI・GCM－Ⅰ）（予報研究部，1984）
A Description of the MRI Atmospheric General Circulation Model (The MRI・GCM－Ⅰ). (Forecast Research Division, 1984)

第 14 号　台風の構造の変化と移動に関する研究－台風 7916 の一生－（台風研究部，1985）
A Study on the Changes of the Three - Dimensional Structure and the Movement Speed of the Typhoon through its Life Time. (Typhoon Research Division, 1985)

第 15 号　波浪推算モデル MRI と MRI－Ⅱの相互比較研究－計算結果図集－（海洋気象研究部，1985）
An Intercomparison Study between the Wave Models MRI and MRI－Ⅱ －A Compilation of Results－ (Oceanographical Research Division, 1985)

第 16 号　地震予知に関する実験的及び理論的研究（地震火山研究部，1985）
Study on Earthquake Prediction by Geophysical Method. (Seismology and Volcanology Research Division, 1985)

第 17 号　北半球地上月平均気温偏差図（予報研究部，1986）
Maps of Monthly Mean Surface Temperature Anomalies over the Northern Hemisphere for 1891－1981. (Forecast Research Division, 1986)

第 18 号　中層大気の研究（高層物理研究部・気象衛星研究部・予報研究部・地磁気観測所，1986）
Studies of the Middle Atmosphere. (Upper Atmosphere Physics Research Division, Meteorological Satellite Research Division, Forecast Research Division, MRI and the Magnetic Observatory, 1986)

第 19 号　ドップラーレーダによる気象・海象の研究（気象衛星研究部・台風研究部・予報研究部・応用気象研究部・海洋研究部，1986）
Studies on Meteorological and Sea Surface Phenomena by Doppler Radar. (Meteorological Satellite Research Division, Typhoon Research Division, Forecast Research Division, Applied Meteorology Research Division, and Oceanographical Research Division, 1986)

第 20 号　気象研究所対流圏大気大循環モデル（MRI・GCM－Ⅰ）による 12 年間分の積分（予報研究部，1986）
Mean Statistics of the Tropospheric MRI・GCM－Ⅰbased on 12－year Integration. (Forecast Research Division, 1986)

第 21 号　宇宙線中間子強度 1983－1986（高層物理研究部，1987）
Multi－Directional Cosmic Ray Meson Intensity 1983－1986. (Upper Atmosphere Physics Research Division, 1987)

第 22 号　静止気象衛星「ひまわり」画像の噴火噴煙データに基づく噴火活動の解析に関する研究（地震火山研究部，1987）
Study on Analysis of Volcanic Eruptions based on Eruption Cloud Image Data obtained by the Geostationary Meteorological satellite (GMS). (Seismology and Volcanology Research Division, 1987)
第 23 号　オホーツク海海洋気候図（篠原吉雄・四竈信行，1988）
Marine Climatological Atlas of the sea of Okhotsk. (Y. Shinohara and N. Shikama, 1988)
第 24 号　海洋大循環モデルを用いた風の応力異常に対する太平洋の応答実験（海洋研究部，1989）
Response Experiment of Pacific Ocean to Anomalous Wind Stress with Ocean General Circulation Model. (Oceanographical Research Division, 1989)
第 25 号　太平洋における海洋諸要素の季節平均分布（海洋研究部，1989）
Seasonal Mean Distribution of Sea Properties in the Pacific. (Oceanographical Research Division, 1989)
第 26 号　地震前兆現象のデータベース（地震火山研究部，1990）
Database of Earthquake Precursors. (Seismology and Volcanology Research Division, 1990)
第 27 号　沖縄地方における梅雨期の降水システムの特性（台風研究部，1991）
Characteristics of Precipitation Systems During the Baiu Season in the Okinawa Area. (Typhoon Research Division, 1991)
第 28 号　気象研究所・予報研究部で開発された非静水圧モデル（猪川元興・斉藤和雄，1991）
Description of a Nonhydrostatic Model Developed at the Forecast Research Department of the MRI. (M. Ikawa and K. Saito, 1991)
第 29 号　雲の放射過程に関する総合的研究（気候研究部・物理気象研究部・応用気象研究部・気象衛星・観測システム研究部・台風研究部，1992）
A Synthetic Study on Cloud－Radiation Processes. (Climate Research Department, Physical Meteorology Research Department, Applied Meteorology Research Department, Meteorological Satellite and Observation System Research Department, and Typhoon Research Department, 1992)
第 30 号　大気と海洋・地表とのエネルギー交換過程に関する研究（三上正男・遠藤昌宏・新野　宏・山崎孝治，1992）
Studies of Energy Exchange Processes between the Ocean－Ground Surface and Atmosphere. (M. Mikami, M. Endoh, H. Niino, and K. Yamazaki, 1992)
第 31 号　降水日の出現頻度からみた日本の季節推移－30 年間の日降水量資料に基づく統計－（秋山孝子，1993）
Seasonal Transition in Japan, as Revealed by Appearance Frequency of Precipitating-Days. －Statistics of Daily Precipitation Data During 30 Years－(T. Akiyama, 1993)
第 32 号　直下型地震予知に関する観測的研究（地震火山研究部，1994）
Observational Study on the Prediction of Disastrous Intraplate Earthquakes. (Seismology and Volcanology Research Department, 1994)
第 33 号　各種気象観測機器による比較観測（気象衛星・観測システム研究部，1994）
Intercomparisons of Meteorological Observation Instruments. (Meteorological Satellite and Observation System Research Department, 1994)
第 34 号　硫黄酸化物の長距離輸送モデルと東アジア地域への適用（応用気象研究部，1995）
The Long－Range Transport Model of Sulfur Oxides and Its Application to the East Asian Region. (Applied Meteorology Research Department, 1995)
第 35 号　ウインドプロファイラーによる気象の観測法の研究（気象衛星・観測システム研究部，1995）
Studies on Wind Profiler Techniques for the Measurements of Winds. (Meteorological Satellite and Observation System Research Department, 1995)
第 36 号　降水・落下塵中の人工放射性核種の分析法及びその地球化学的研究（地球化学研究部，1996）
Geochemical Studies and Analytical Methods of Anthropogenic Radionuclides in Fallout Samples. (Geochemical Research Department, 1996)
第 37 号　大気と海洋の地球化学的研究（1995 年及び 1996 年）（地球化学研究部，1998）
Geochemical Study of the Atmosphere and Ocean in 1995 and 1996. (Geochemical Research Department, 1998)
第 38 号　鉛直２次元非線形問題（金久博忠，1999）
Vertically 2-dmensional Nonlinear Problem (H. Kanehisa, 1999)
第 39 号　客観的予報技術の研究（予報研究部，2000）
Study on the Objective Forecasting Techniques（Forecast Research Department, 2000）
第 40 号　南関東地域における応力場と地震活動予測に関する研究（地震火山研究部，2000）
Study on Stress Field and Forecast of Seismic Activity in the Kanto Region（Seismology and Volcanology Research Department, 2000）
第 41 号　電量滴定法による海水中の全炭酸濃度の高精度分析および大気中の二酸化炭素と海水中の全炭酸の放射性炭素同位体比の測定（石井雅男・吉川久幸・松枝秀和，2000）
Coulometric Precise Analysis of Total Inorganic Carbon in Seawater and Measurements of Radiocarbon for the Carbon Dioxide in the Atmosphere and for the Total Inorganic Carbon in Seawater（I.Masao, H.Y.Inoue and H.Matsueda, 2000）
第 42 号　気象研究所／数値予報課統一非静力学モデル（斉藤和雄・加藤輝之・永戸久喜・室井ちあし，2001）
Documentation of the Meteorological Research Institute / Numerical Prediction Division Unified Nonhydrostatic Model (Kazuo Saito, Teruyuki Kato, Hisaki Eito and Chiashi Muroi，2001)
第 43 号　大気および海水中のクロロフルオロカーボン類の精密測定と気象研究所クロロフルオロカーボン類標準ガスの確立（時枝隆之・井上(吉川)久幸，2004）
Precise measurements of atmospheric and oceanic chlorofluorocarbons and MRI chlorofluorocarbons calibration scale

(Takayuki Tokieda and Hisayuki Y. Inoue，2004)

第 44 号　PostScript コードを生成する描画ツール"PLOTPS"マニュアル（加藤輝之，2004）
Documentation of "PLOTPS": Outputting Tools for PostScript Code (Teruyuki Kato，2004)

第 45 号　気象庁及び気象研究所における二酸化炭素の長期観測に使用された標準ガスのスケールとその安定性の再評価に関する調査・研究（松枝秀和・須田一人・西岡佐喜子・平野礼朗・澤　庸介・坪井一寛・堤　之智・神谷ひとみ・根本和宏・長井秀樹・吉田雅司・岩野園城・山本　治・森下秀昭・鎌田匡俊・和田　晃，2004）
Re-evaluation for scale and stability of CO_2 standard gases used as long-term observations at the Japan Meteorological Agency and the Meteorological Research Institute (Hidekazu Matsueda, Kazuto Suda, Sakiko Nishioka, Toshirou Hirano, Yousuke, Sawa, Kazuhiro Tuboi, Tsutumi, Hitomi Kamiya, Kazuhiro Nemoto, Hideki Nagai, Masashi Yoshida, Sonoki Iwano, Osamu Yamamoto, Hideaki Morishita, Kamata, Akira Wada，2004)

第 46 号　地震発生過程の詳細なモデリングによる東海地震発生の推定精度向上に関する研究（地震火山研究部, 2005）
A Study to Improve Accuracy of Forecasting the Tokai Earthquake by Modeling the Generation Processes (Seismology and Volcanology Research Department, 2005)

第 47 号　気象研究所共用海洋モデル（MRI.COM）解説（海洋研究部, 2005）
Meteorological Research Institute Community Ocean Model (MRI.COM) Manual (Oceanographical Research Department, 2005)

第 48 号　日本海降雪雲の降水機構と人工調節の可能性に関する研究（物理気象研究部・予報研究部, 2005）
Study of Precipitation Mechanisms in Snow Clouds over the Sea of Japan and Feasibility of Their Modification by Seeding (Physical Meteorology Research Department, Forecast Research Department, 2005)

第 49 号　2004 年日本上陸台風の概要と環境場（台風研究部, 2006）
Summary of Landfalling Typhoons in Japan, 2004 (Typhoon Research Department, 2006)

第 50 号　栄養塩測定用海水組成標準の 2003 年国際共同実験報告（青山道夫, 2006）
2003 Intercomparison Exercise for Reference Material for Nutrients in Seawater in a Seawater Matrix (Michio Aoyama, 2006)

第 51 号　大気および海水中の超微量六フッ化硫黄(SF_6)の測定手法の高度化と SF_6 標準ガスの長期安定性の評価（時枝隆之、石井雅男、斉藤 秀、緑川 貴, 2007）
Highly developed precise analysis of atmospheric and oceanic sulfur hexafluoride (SF_6) and evaluation of SF_6 standard gas stability (Takayuki Tokieda, Masao Ishii, Shu Saito and Takashi Midorikawa, 2007)

第 52 号　地球温暖化による東北地方の気候変化に関する研究（仙台管区気象台, 環境・応用気象研究部, 2008）
Study of Climate Change over Tohoku District due to Global Warming (Sendai District Meteorological Observatory, Atmospheric Environment and Applied Meteorology Research Department, 2008)

第 53 号　火山活動評価手法の開発研究（地震火山研究部, 2008）
Studies on Evaluation Method of Volcanic Activity (Seismology and Volcanology Research Department, 2008)

第 54 号　日本における活性炭冷却捕集およびガスクロ分離による気体計数システムによる ^{85}Kr の測定システムの構築および 1995 年から 2006 年の測定結果（青山道夫, 藤井憲治, 廣瀬勝己, 五十嵐康人, 磯貝啓介, 新田 済, Hartmut Sartorius, Clemens Schlosser, Wolfgang Weiss, 2008）
Establishment of a cold charcoal trap-gas chromatography-gas counting system for ^{85}Kr measurements in Japan and results from 1995 to 2006 (Michio Aoyama, Kenji Fujii, Katsumi Hirose, Yasuhito Igarashi, Keisuke Isogai, Wataru Nitta, Hartmut Sartorius, Clemens Schlosser, Wolfgang Weiss, 2008)

第 55 号　長期係留による 4 種類の流速計観測結果の比較（中野俊也, 石崎 廣, 四竈信行, 2008）
Comparison of Data from Four Current Meters Obtained by Long-Term Deep-Sea Moorings (Toshiya Nakano, Hiroshi Ishizaki and Nobuyuki Shikama, 2008)

第 56 号　CMIP3 マルチモデルアンサンブル平均を利用した将来の海面水温・海氷分布の推定（水田 亮, 足立恭将, 行本誠史, 楠 昌司, 2008）
Estimation of the Future Distribution of Sea Surface Temperature and Sea Ice Using the CMIP3 Multi-model Ensemble Mean (Ryo Mizuta, Yukimasa Adachi, Seiji Yukimoto and Shoji Kusunoki, 2008)

第 57 号　閉流路中のフローセルを用いた分光光度法自動分析装置による海水の高精度 pH_T 測定（斉藤 秀, 石井雅男, 緑川 貴, 井上（吉川）久幸, 2008）
Precise Spectrophotometric Measurement of Seawater pH_T with an Automated Apparatus using a Flow Cell in a Closed Circuit（Shu Saito, Masao Ishii, Takashi Midorikawa and Hisayuki Y. Inoue, 2008）

第58号　栄養塩測定用海水組成標準の2006年国際共同実験報告(青山道夫,J. Barwell-Clarke, S. Becker, M. Blum, Braga E.S., S. C. Coverly, E. Czobik, I. Dahllöf, M. Dai, G. O Donnell, C. Engelke, Gwo-Ching Gong, Gi-Hoon Hong, D. J. Hydes, Ming-Ming Jin, 葛西広海, R. Kerouel, 清本容子, M. Knockaert, N. Kress, K. A. Krogslund, 熊谷正光, S. Leterme, Yarong Li, 増田真次, 宮尾 孝, T. Moutin, 村田昌彦, 永井直樹, G. Nausch, A. Nybakk, M. K. Ngirchechol, 小川浩史, J. van Ooijen, 太田秀和, J. Pan, C. Payne, O. Pierre-Duplessix, M. Pujo-Pay, T. Raabe, 齊藤一浩, 佐藤憲一郎, C. Schmidt, M. Schuett, T. M. Shammon, J. Sun, T. Tanhua, L. White, E.M.S. Woodward, P. Worsfold, P. Yeats, 芳村 毅, A. Youénou, Jia-Zhong Zhang, 2008）
2006 Inter-laboratory Comparison Study for Reference Material for Nutrients in Seawater（M. Aoyama, J. Barwell-Clarke, S. Becker, M. Blum, Braga E. S., S. C. Coverly, E. Czobik, I. Dahllöf, M. H. Dai, G. O. Donnell, C. Engelke, G. C. Gong, Gi-Hoon Hong, D. J. Hydes, M. M. Jin, H. Kasai, R. Kerouel, Y. Kiyomono, M. Knockaert, N. Kress, K. A. Krogslund, M. Kumagai, S. Leterme, Yarong Li, S. Masuda, T. Miyao, T. Moutin, A. Murata, N. Nagai, G. Nausch, M. K. Ngirchechol, A. Nybakk, H. Ogawa, J. van Ooijen, H. Ota, J. M. Pan, C. Payne, O. Pierre-Duplessix, M. Pujo-Pay, T. Raabe, K. Saito, K. Sato, C. Schmidt, M. Schuett, T. M. Shammon, J. Sun, T. Tanhua, L. White, E.M.S. Woodward, P. Worsfold, P. Yeats, T.

Yoshimura, A. Youénou, J. Z. Zhang, 2008）

第 59 号　気象研究所共用海洋モデル(MRI.COM)第 3 版解説（辻野博之, 本井達夫, 石川一郎, 平原幹俊, 中野英之, 山中吾郎, 安田珠幾, 石崎廣（気象研究所海洋研究部）, 2010）

Reference manual for the Meteorological Research Institute Community Ocean Model (MRI.COM) Version 3（Hiroyuki Tsujino, Tatsuo Motoi, Ichiro Ishikawa, Mikitoshi Hirabara, Hideyuki Nakano, Goro Yamanaka, Tamaki Yasuda, and Hiroshi Ishizaki (Oceanographic Research Department), 2010）

第 60 号　栄養塩測定用海水組成標準の 2008 年国際共同実験報告（青山道夫, Carol Anstey, Janet Barwell-Clarke, François Baurand, Susan Becker, Marguerite Blum, Stephen C. Coverly, Edward Czobik, Florence D’amico, Ingela Dahllöf, Minhan Dai, Judy Dobson, Magali Duval, Clemens Engelke, Gwo-Ching Gong, Olivier Grosso, 平山篤史, 井上博敬, 石田雄三, David J. Hydes, 葛西広海, Roger Kerouel, Marc Knockaert, Nurit Kress, Katherine A. Krogslund, 熊谷正光, Sophie C. Leterme, Claire Mahaffey, 光田均, Pascal Morin, Thierry Moutin, Dominique Munaron, 村田昌彦, Günther Nausch, 小川浩史, Jan van Ooijen, Jianming Pan, Georges Paradis, Chris Payne, Olivier Pierre-Duplessix, Gary Prove, Patrick Raimbault, Malcolm Rose, 齊藤一浩, 斉藤宏明, 佐藤憲一郎, Cristopher Schmidt, Monika Schütt, Theresa M. Shammon, Solveig Olafsdottir, Jun Sun, Toste Tanhua, Sieglinde Weigelt-Krenz, Linda White, E. Malcolm. S. Woodward, Paul Worsfold, 芳村毅, Agnès Youénou, Jia-Zhong Zhang, 2010）

2008 Inter-laboratory Comparison Study of a Reference Material for Nutrients in Seawater（青山道夫, Carol Anstey, Janet Barwell-Clarke, François Baurand, Susan Becker, Marguerite Blum, Stephen C. Coverly, Edward Czobik, Florence D’amico, Ingela Dahllöf, Minhan Dai, Judy Dobson, Magali Duval, Clemens Engelke, Gwo-Ching Gong, Olivier Grosso, 平山篤史, 井上博敬, 石田雄三, David J. Hydes, 葛西広海, Roger Kerouel, Marc Knockaert, Nurit Kress, Katherine A. Krogslund, 熊谷正光, Sophie C. Leterme, Claire Mahaffey, 光田均, Pascal Morin, Thierry Moutin, Dominique Munaron, 村田昌彦, Günther Nausch, 小川浩史, Jan van Ooijen, Jianming Pan, Georges Paradis, Chris Payne, Olivier Pierre-Duplessix, Gary Prove, Patrick Raimbault, Malcolm Rose, 齊藤一浩, 斉藤宏明, 佐藤憲一郎, Cristopher Schmidt, Monika Schütt, Theresa M. Shammon, Solveig Olafsdottir, Jun Sun, Toste Tanhua, Sieglinde Weigelt-Krenz, Linda White, E. Malcolm. S. Woodward, Paul Worsfold, 芳村毅, Agnès Youénou, Jia-Zhong Zhang, 2010）

第 61 号　強雨をもたらす線状降水帯の形成機構等の解明及び降水強度・移動速度の予測に関する研究（大阪管区気象台・彦根地方気象台・京都地方気象台・奈良地方気象台・和歌山地方気象台・神戸海洋気象台・松江地方気象台・鳥取地方気象台・舞鶴海洋気象台・広島地方気象台・徳島地方気象台・予報研究部, 2010）

Studies on formation process of line-shaped rainfall systems and predictability of rainfall intensity and moving speed（Osaka District Meteorological Observatory, Hikone Local Meteorological Observatory, Kyoto Local Meteorological Observatory, Nara Local Meteorological Observatory, Wakayama Local Meteorological Observatory, Kobe Marine Observatory, Matsue Local Meteorological Observatory, Tottori Local Meteorological Observatory, Maizuru Marine Observatory, Hiroshima Local Meteorological Observatory, Tokushima Local Meteorological Observatory AND Forecast Research Department, 2010）

第 62 号　WWRP 北京オリンピック 2008 予報実証/研究開発プロジェクト（齊藤和雄, 國井勝, 原昌弘, 瀬古弘, 原旅人, 山口宗彦, 三好建正, 黄偉健, 2010）

WWRP Beijing Olympics 2008 Forecast Demonstration/Research and Development Project (B08FDP/RDP)（Kazuo Saito, Masaru Kunii, Masahiro Hara, Hiromu Seko, Tabito Hara, Munehiko Yamaguchi, Takemasa Miyoshi and Wai-kin Wong, 2010）

第 63 号　東海地震の予測精度向上及び東南海・南海地震の発生準備過程の研究（地震火山研究部, 2011）

Improvement in prediction accuracy for the Tokai earthquake and research of the preparation process of the Tonankai and the Nankai earthquakes (Seismology and Volcanology Research Department, 2011)

第 64 号　気象研究所地球システムモデル第 1 版（MRI-ESM1）―モデルの記述―（行本誠史, 吉村裕正, 保坂征宏, 坂見智法, 辻野博之, 平原幹俊, 田中泰宙, 出牛真, 小畑淳, 中野英之, 足立恭将, 新藤永樹, 鍛冶将吉, 尾瀬智昭, 鬼頭昭雄, 2011）

Meteorological Research Institute-Earth System Model Version 1 (MRI-ESM1) — Model Description —（Seiji Yukimoto, Hiromasa Yoshimura, Masahiro Hosaka, Tomonori Sakami, Hiroyuki Tsujino, Mikitoshi Hirabara, Taichu Y. Tanaka, Makoto Deushi, Atsushi Obata, Hideyuki Nakano, Yukimasa Adachi, Eiki Shindo, Shoukichi Yabu, Tomoaki Ose and Akio Kitoh, 2011)

第 65 号　東南アジア地域の気象災害軽減国際共同研究（斉藤和雄, 黒田徹, 林修吾, 瀬古弘, 國井勝, 小司禎教, 上野充, 川畑拓矢, 余田成男, 大塚成徳, Nurjanna Joko Trilaksono, 許智揚, 古関俊也, Le Duc, Kieu Thi Xin, 黄偉健、Krushna Chandra Gouda, 2011）

International Research for Prevention and Mitigation of Meteorological Disasters in Southeast Asia (Kazuo Saito, Tohru Kuroda, Syugo Hayashi, Hiromu Seko, Masaru Kunii, Yoshinori Shoji, Mitsuru Ueno, Takuya Kawabata, Shigeo Yoden, Shigenori Otsuka, Nurjanna Joko Trilaksono, Tieh-Yong Koh, Syunya Koseki, Le Duc, Kieu Thi Xin, Wai-Kin Wong and Krushna Chandra Gouda, 2011)

気象研究所技術報告は，1978（昭和53）年の初刊以来,気象研究所が必要の都度発行する刊行物であり，気象研究所の研究計画に基づき実施した研究に関する手法、データ、結果等についてのまとめ、または、すでに公表した研究論文類をとりまとめ総合的報告としたものを掲載する。

気　象　研　究　所　技　術　報　告　　ISSN 0386-4049
第　66　号

平成24年2月　発行

編集兼
発行者　気　象　研　究　所
〒305-0052　茨城県つくば市長峰１－１
TEL(029)853-8535

印　刷　者　朝日印刷株式会社　つくば支社
〒305-8519　茨城県つくば市東2-11-15
TEL(029)851-1188